NATIONAL AERONAUTICS AND SPACE ADMINISTRATION

Technical Report No. 32-982

Experimental Investigation of a Confined, Jet-Driven Water Vortex

E. J. Roschke

JET PROPULSION LABORATORY
CALIFORNIA INSTITUTE OF TECHNOLOGY
PASADENA, CALIFORNIA

October 1, 1966

NATIONAL AERONAUTICS AND SPACE ADMINISTRATION

Technical Report No. 32-982

Experimental Investigation of a Confined, Jet-Driven Water Vortex

E. J. Roschke

Approved by:

D. R. Bartz, *Manager*
Research and Advanced Concepts Section

JET PROPULSION LABORATORY
CALIFORNIA INSTITUTE OF TECHNOLOGY
PASADENA, CALIFORNIA

October 1, 1966

Prepared Under Contract No. NAS 7-100
National Aeronautics & Space Administration

CONTENTS

TABLES

FIGURES

FIGURES (Cont'd)

ABSTRACT

For some years, the use of a confined, vortex flow has been proposed as one possible method of achieving nuclear fuel containment in the so-called gaseous-core (or cavity) nuclear reactor. It is recognized that fluid dynamic considerations may impose severe restrictions on a reactor of this type, as conceived for use in a nuclear propulsion scheme. One factor that may limit the potential capability of the vortex for fuel containment and separation is the length-to-diameter ratio (aspect ratio) of the vortex tube. This report deals with some of the effects on a confined, vortex flow produced by varying the aspect ratio. Investigation of a vortex flow of water within a right, circular cylinder, having a single, circular exit-hole centrally located in one end wall was accomplished primarily by means of static pressure measurements made on the closed end-wall. This vortex tube had a fixed diameter D, but a variable length L, such that aspect ratio variations in the range $0 < L/D < 12$ were obtainable. Experiments were conducted in the radial Reynolds number range $40 < Re_r < 1100$, using several exit-hole diameters of different size. Radial distributions of static pressure measured at the closed end-wall are presented for a variety of conditions in such a way as to bring out the effects of L/D while holding other parameters fixed. Tangential velocity distributions and angular momentum distributions were obtained by graphical differentiation of the static pressure distributions. Typical values of the jet recovery factor, the tangential Reynolds number, and the cylindrical-wall skin friction coefficient were inferred from pressure data. Because of the limited accuracy of the data, it was possible to establish only trends, but they are sufficiently well-determined as to show clearly the importance of aspect ratio on vortex flows of this type. One significant effect produced by an increasing L/D is a corresponding reduction in the size of the vortex core. It appears that increases in aspect ratio to increasingly larger values would have the adverse effect of producing vortexes of decreasing strength, if the pressure at the cylindrical wall were held fixed. This possibility would impose severe restrictions on performance of multiple vortex-tube gas-core reactors that rely on diffusion-controlled nuclear-fuel containment and require vortex flows of high strength.

I. INTRODUCTION

Many practical and potential applications of swirling, rotating and vortex-like flows have, in recent years, stimulated research in a classical field once largely of academic interest. Such diverse applications as mass and energy separation, flow and heat transfer in various types of industrial and laboratory equipment, propulsion, flow dynamics of aircraft, and studies of various natural phenomena of interest to meteorologists, geophysicists, and astronomers are broadly discussed (Refs. 1-3). In the last six years, vortex flows have found application in nuclear propulsion (Refs. 4-6), magnetohydrodynamic power generation (Refs. 7, 8), and electric arc stabilization (Refs. 9, 10).

Interest in the gaseous-core reactor as an element of a nuclear propulsion scheme was the motivation for research in vortex flows at the Jet Propulsion Laboratory. Subsequently, all experimental research was of a fluid mechanics nature (Refs. 11, 12) because it was felt that the feasibility of such a propulsion concept would depend strongly on flow characteristics of the vortex tube. Kendall's work (Ref. 11) demonstrated important aspects of this type flow, e.g., the strong influence of end-wall boundary layers on a confined, vortex flow. Pivirotto (Ref. 12) made radial-distribution measurements of relative species concentration in a binary gaseous vortex. Pivirotto's work is of great importance, as it has bearing on the separation capabilities of a vortex flow, a feature of direct consequence to the gaseous-core reactor concept. The diffusion scheme (Ref. 4) indicates high-strength vortex flows are required for producing adequate retention and separation of nuclear fuel. (High-strength could, for example, be characterized by high tangential velocity or by large, radial pressure gradient.) Practical applications of the diffusion scheme in a propulsion device would probably result in an array of many small-diameter, slender vortex tubes, rather than a single, large cavity of relatively short proportion. Thus, relative slenderness (aspect ratio) is one of the many factors that could have important effect on the strength of the vortex and its intended performance. Partly, this is because flow in a vortex tube is highly three-dimensional, rather than two-dimensional (as assumed in Ref. 4).

The experiments reported here, an extension of Kendall's water vortex studies, were intended to supplement the gas vortex work of Pivirotto. A water vortex was selected because of the ease and desirability of visualizing flow that might retain principal features of a gas vortex. The purpose was to investigate, both qualitatively and quantitatively, effects of aspect ratio on flow in a confined, jet-driven vortex tube. The effects on vortex strength and effects on secondary flow structure were of particular interest. Aspect ratio is defined as the length-to-diameter ratio (L/D) of a vortex tube. Little information of L/D effects on flows of this type appears in the literature. This report deals with the quantitative aspects of the experimental work: (1) static pressure distributions measured at the closed end wall of the vortex tube — a simple right, circular cylinder, having an exit-hole centrally located in one end-wall for various conditions of mass rate of flow, aspect ratio, and exit-hole diameter, (2) tangential velocity distributions determined from static pressure distributions, and (3) additional information inferred from velocity data, e.g., jet-recovery factor, cylindrical wall-friction, and tangential Reynolds number. Flow visualization studies, conducted in support of quantitative work, were accomplished by observing motions of colored dyes injected at discrete locations in the vortex tube (Ref. 13).

Experimental work on swirling flow of water, excluding a large body of work in the annular gap between rotating cylinders, is well represented (Refs. 13-31). Perhaps the most striking single impression on perusing these references is the large number of complicated secondary flow patterns observed for a wide variety of experimental conditions and apparatus. References 18-22, 26, and 30, discuss observations of water flow with an air core present. To the author's knowledge, Refs. 22 and 24 present the only available detailed data (for rotating water flows) obtained by probing the flow; their applications are to swirling-pipe flow and vortex-chamber flow, respectively. Reference 25 presents an interesting method of generating a vortex-like flow without benefit of guide-vanes or sinks, and with zero net flow. The apparatus and experiment of Ref. 27 is very similar to the work reported here. The work presented in Ref. 29 for a toroidal vortex having no end walls was discontinued, as the device exhibited no clear advantage over the conventional vortex tube (Ref. 30). The vortex tube (Ref. 30) is treated in detail here. This tube was conventional in every way, except that it employed a long exit tube attached to the orifice. For this reason, the work reported in Refs. 16, 19, 22, 26, and 28 was of interest.

Since the 1951 paper of Einstein and Li (Ref. 14), steady progress has been made in the analytical description of laminar, incompressible vortex flows (Refs. 16,

17, and 32-41). These analyses pertain to both infinite and to bounded or confined vortex flows. Closed-form solutions for certain two-dimensional vortex flows are available (Refs. 14, 34, 37). Although these solutions are too restrictive, and not physically realistic, they serve as convenient models with which experimental velocity distributions may be compared — models certainly better than the traditional potential flow type. Reference 37 gives a closed-form solution for static pressure in the annular region exterior to the viscous core region (Ref. 14). Three-dimensional numerical solutions for certain special cases are available (Refs. 32, 33, 35, 36, 38, and 39). The foregoing solutions all fail because of the arbitrary and restrictive assumptions made concerning boundary conditions and/or three-dimensional characteristics of the flow. In addition, applications to confined vortex flows are limited because of negligible attention given to end-wall boundary layers and their interactions with the primary vortex flow. The most general of all solutions to date are incorporated in the work of Lewellen (Refs. 40, 41).

Realization of importance of end-wall boundary layer interactions in confined vortex flows has stimulated research on boundary layers generated by rotating flows on fixed surfaces (Refs. 42-47). A further step, recently taken (Ref. 48), consists of an attempt to analyze the interaction problem by combining the work of Refs. 40, 45. Those results, which are thought to preserve essential characteristics observed in real vortex flows, show that three-dimensional adjustments in a vortex flow tend to occur in such a way as to force two-dimensionality in the tangential velocity. These adjustments give rise to thin shear regions observed in real vortex flows.

All laminar vortex solutions seem to contain the radial Reynolds number directly or indirectly. There is no clear way to specify Re_r because of boundary condition difficulties and/or the effects of turbulence. Presently, a controversy exists as to whether the effects of mass flow diversion into the end-wall boundary layers or turbulence is dominantly responsible for degradation of circulation ($\Gamma = 2\pi vr$) experimentally observed in confined vortex flows. Authors of Refs. 5, 48 and 49 favor boundary layer effects, whereas authors of Refs. 7, 11 and 50 favor turbulence effects. A small amount of data taken in a liquid cyclone, using polarographic methods (Ref. 51), appears to corroborate certain of the results of Ref. 50.

II. DESCRIPTION OF APPARATUS AND INSTRUMENTATION

A schematic view of the vortex tube and its principal dimensions is shown in Fig. 1; Fig. 2 is a photograph of the assembled vortex apparatus. The vortex tube, fabricated from a length of plexiglass pipe, having a nominal 4 in. ID, was placed within a long container of square cross-section. Container space external to the vortex tube served as a plenum chamber. Figure 1 illustrates the driving-jet orifices drilled through the wall of the vortex tube. Two rows of orifices, located 180 deg apart, consisted of individual 0.0625-in.-diameter holes, spaced at 0.25-in. intervals along the entire length of the tube. Length-to-diameter ratio of the driving-jet orifices was approximately 7.6. Water, introduced into the plenum chamber at twelve separate locations, entered the vortex tube through the orifices (thereby producing the driving jets), passed through an exit hole centrally located in one end wall, then discharged to ambient conditions through an exit tube. This flow system is illustrated schematically (Fig. 3). Ordinary laboratory water, with two stages of pressure regulation, was used. Weight flow rate was measured by three calibrated rotameters (Fig. 3). Provision was made to measure the supply water temperature and the barometric pressure. Most of the experimental work was conducted using a length of flexible tubing to convey water from the exit tube to an open drain (Fig. 2). Plenum-chamber pressures, up to 50 psig, were obtained safely in this apparatus.

The plenum-chamber container was of welded aluminum construction (top, bottom, and ends) and 1-in. thick plexiglass (side-wall windows) bolted in place and sealed with large O-rings (Fig. 2). The exit hole was located in a piston that could be moved to produce changes in vortex length, and hence, the aspect ratio. Five exit hole sizes were tested; their nominal diameters were ½, 9/16, 11/16, ⅞ and 1 in. Each orifice had a rounded inlet (Fig. 1) of 0.25-in. radius, and each piston was provided with an exit tube, having an ID matched to its exit hole, so that no internal surface discontinuities occurred.

Vortex pistons and end walls were machined from plexiglass. All exit tubes were made from 6-ft lengths

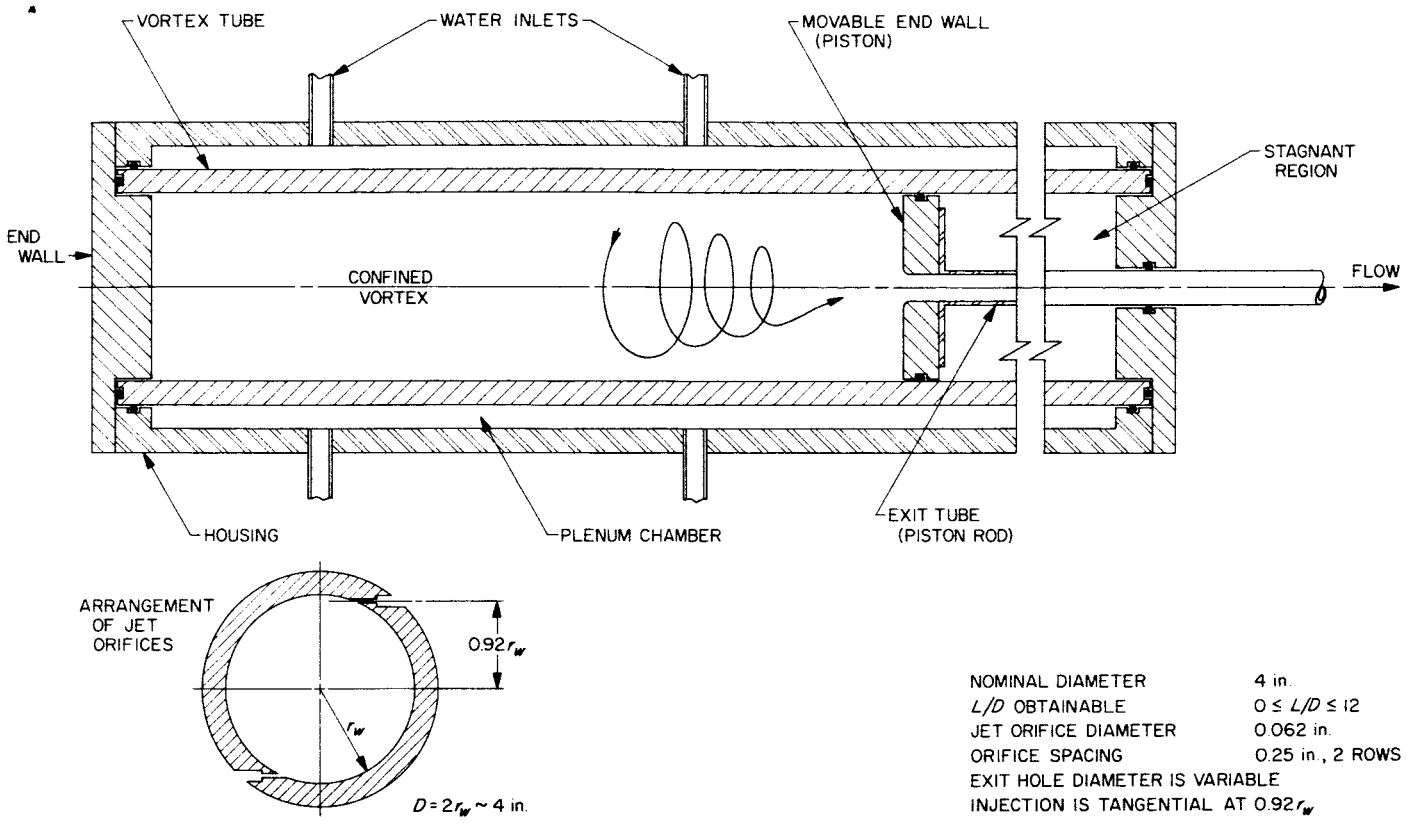

Fig. 1. Schematic arrangement of 4-in.-diam water vortex-tube

of stainless steel tubing, especially selected for straightness and surface smoothness. Thus, the minimum number of exit-tube pipe diameters was 72, in the case of the largest exit hole. Thin sheet metal flow-straighteners, "X"-shaped in cross-section and 10 pipe diameters in length, were mounted in the downstream end of each exit tube. In addition to their use as piston rods, these long exit tubes effectively removed swirl from the vortex discharge, thus preventing atmospheric air from entering the vortex. Air or gas cores generally did occur in the vortex tube; however, their presence was traced to another source which will be discussed later. With the vortex in operation, piston movement was made possible by a manually operated screw-and-gear arrangement mounted external to the vortex tube and adjacent to the exit tube. Aspect ratio settings were made with reference to a scale mounted on the test stand. In Fig. 2, the closed end-wall of the vortex is in the foreground. The exit tube (almost entirely withdrawn from the vortex tube), drive screw, and scale are visible in the right center background. The black box (center foreground) is a portion of light-source apparatus used early in the program for flow visualization.

Various closed end-walls were used depending on application. One was fitted with a series of pressure taps arranged in a spiral array, instead of along a single radius vector, to permit a closer spacing of taps near the center of the end wall, but this arrangement precluded possibility of detecting departures from axisymmetric flow. A rather large pressure-tap diameter (0.030 in.) was selected to reduce response time in measuring static pressure. All pressure taps were connected to a single 16-in.-diameter bourdon-tube pressure gage by a manually-operated selector valve. Several leak-checks of this valve were made over a period of time and operation was determined to be satisfactory. The pressure gage was the compound type, suitable for making vacuum, as well as positive pressure readings. Other end walls included one designed so a small tube could be inserted axially into the vortex at its centerline, also a plain end-wall for flow visualization purposes.

The vortex tube was provided with a series of ports for static wall-pressure measurement, insertion of probes into the flow, and dye injection. Figure 4 illustrates ports

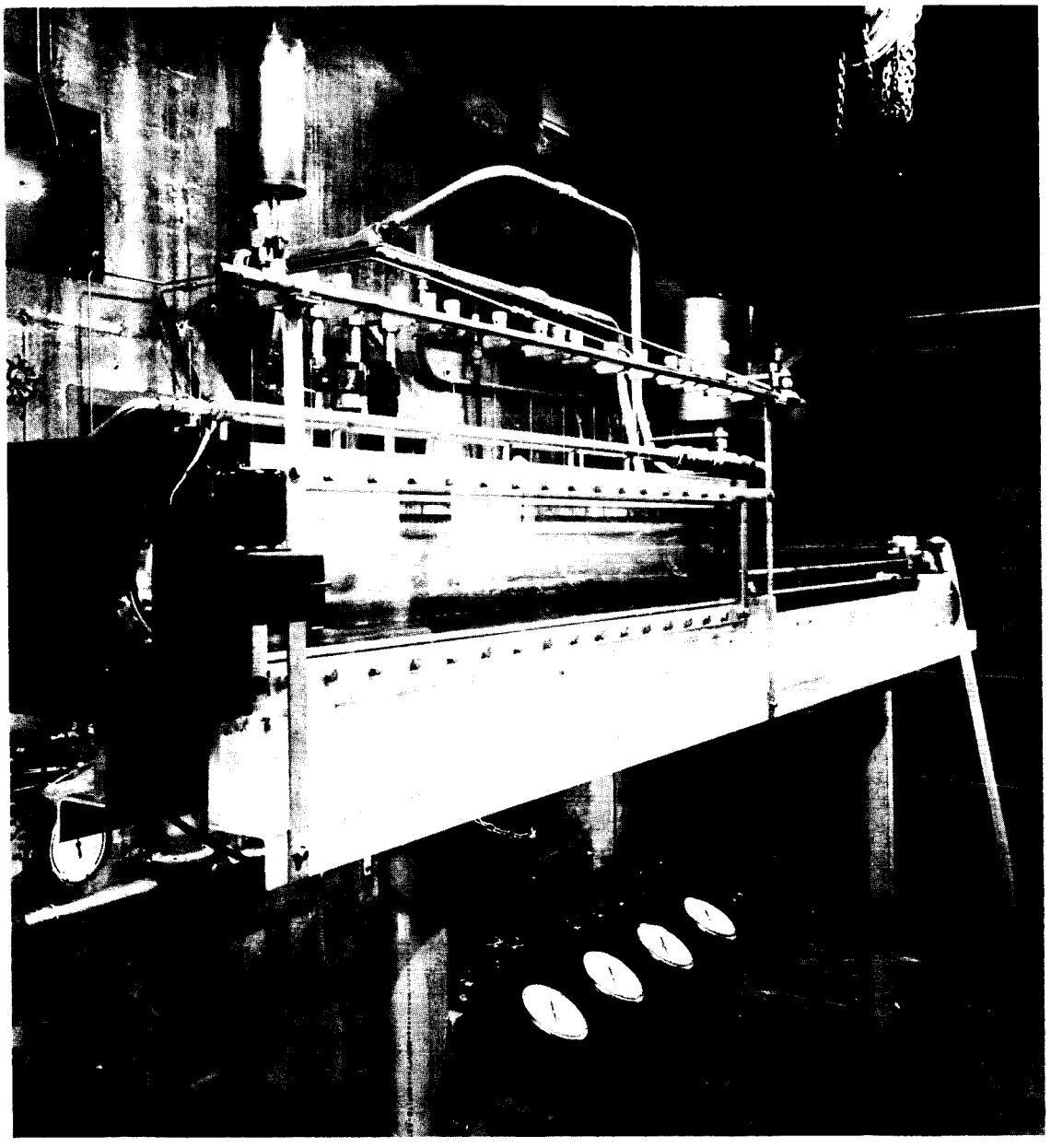

Fig. 2. View of assembled vortex apparatus

designed so that a tube could be passed through the walls of the vortex tube and its container. Ports were spaced axially at approximately 4-in. intervals along the vortex tube, beginning at the closed end-wall. At a later stage of the experimental program, identically matching ports were installed on the lower surface of the vortex tube, 180 deg opposed to the original set. With this arrangement, a small tube, or wire, could be placed entirely across a vortex diameter, with support at either or both ends, as desired. In Fig. 2, the row of small, metal tubes projecting vertically from the top of the vortex container represent the described probes. Static pressure along the cylindrical wall was measured when the sliding probes were withdrawn into the wall of the vortex tube. Pressure differences in the axial direction were indicated on a manometer bank. Carbon tetrachloride was selected as the manometer fluid — the use of oil below water having proved unsatisfactory. Static pressure drop across the driving-jet orifices was measured in a similar manner (i.e., a manometer was connected across a pressure tap in the plenum chamber and a vortex wall tap).

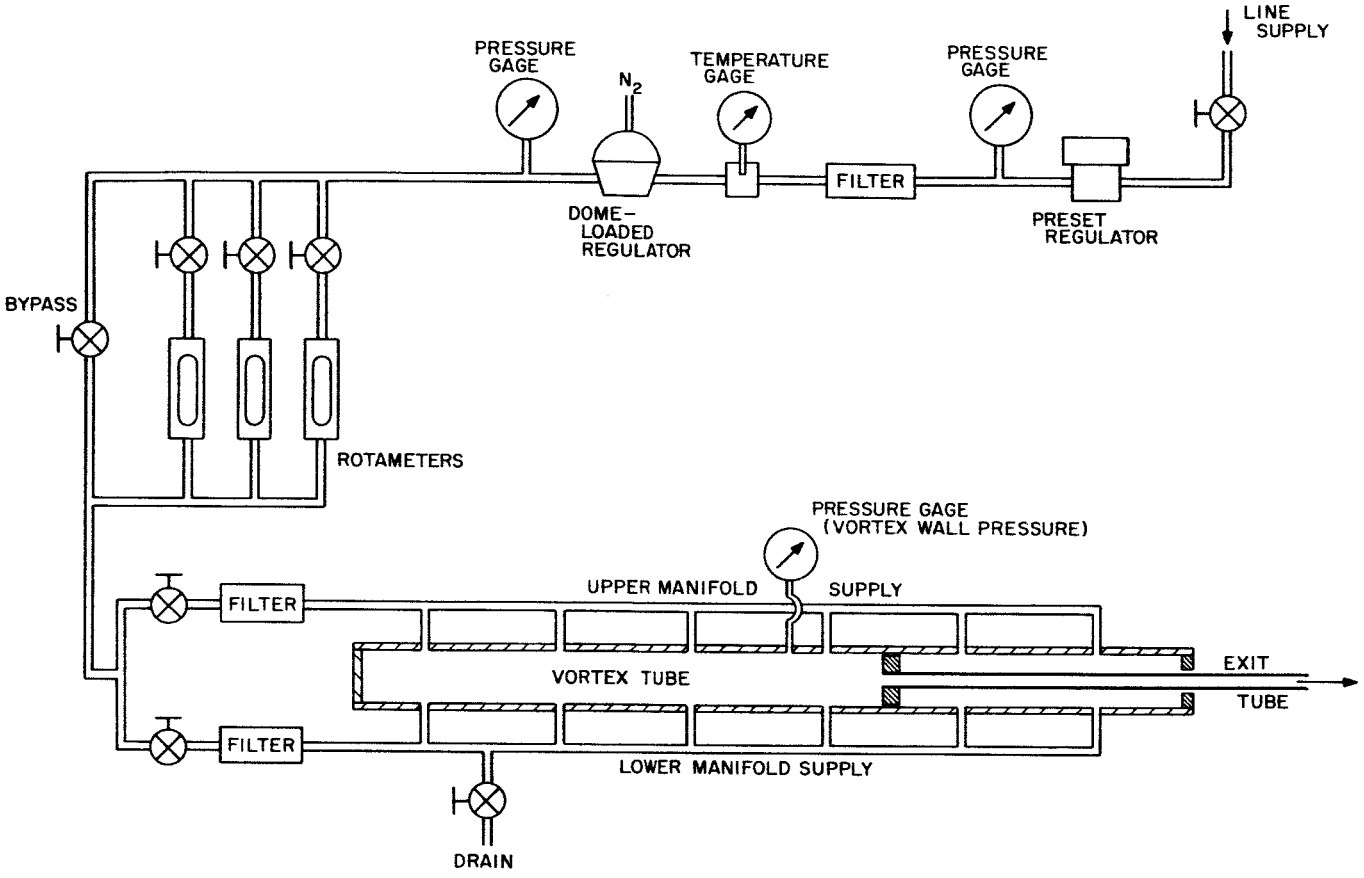

Fig. 3. Schematic flow diagram: water vortex experiment

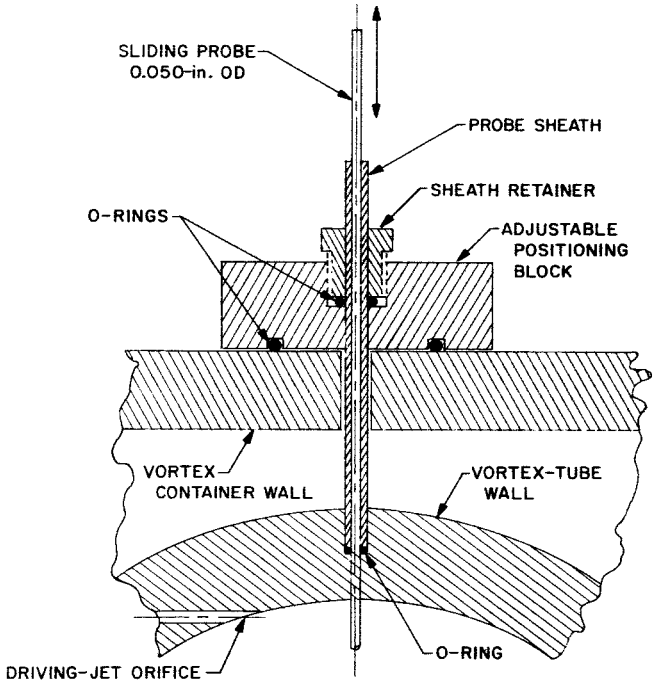

Fig. 4. Port arrangement for insertion of probes into vortex tube

III. VORTEX APPARATUS OPERATION

A. Test Regime: Range of Data Acquisition

The maximum flow rate available to the apparatus was approximately 3.5 lb/sec, or 25 gal/min. Radial distributions of static pressure at the closed end-wall were taken in the range $5 \leq (p_w - p_a) \leq 35$ psig. Corresponding ranges of mass flow rate per unit length ($\dot{m}/L$) and radial Reynolds number are shown (Fig. 5) for the range of aspect ratio L/D. Thus, $40 \leq Re_r \leq 1100$ was the test range. Values of $(p_w - p_a)$, static pressure at the cylindrical wall of the vortex tube, approaching 35 psig were not attainable with the large exit holes at large L/D. With several minor exceptions, only data reported for even values of L/D are presented here.

B. Water Conditions

The rather large flow rates used for long periods of time ruled out the use of a pressurized-reservoir water source. Use of dye in large amounts made application of a pump-powered, closed-loop water system undesirable. Therefore, the alternative was an open system, using laboratory water suitably regulated for pressure (average temperature approximately 68°F). This system (Fig. 3) had several disadvantages which are discussed in this and some following sections. Water conditions on a day-to-day basis were highly variable with respect to inclusion of dirt, gas, and other foreign material. Employment of filters was successful only in removing larger-sized

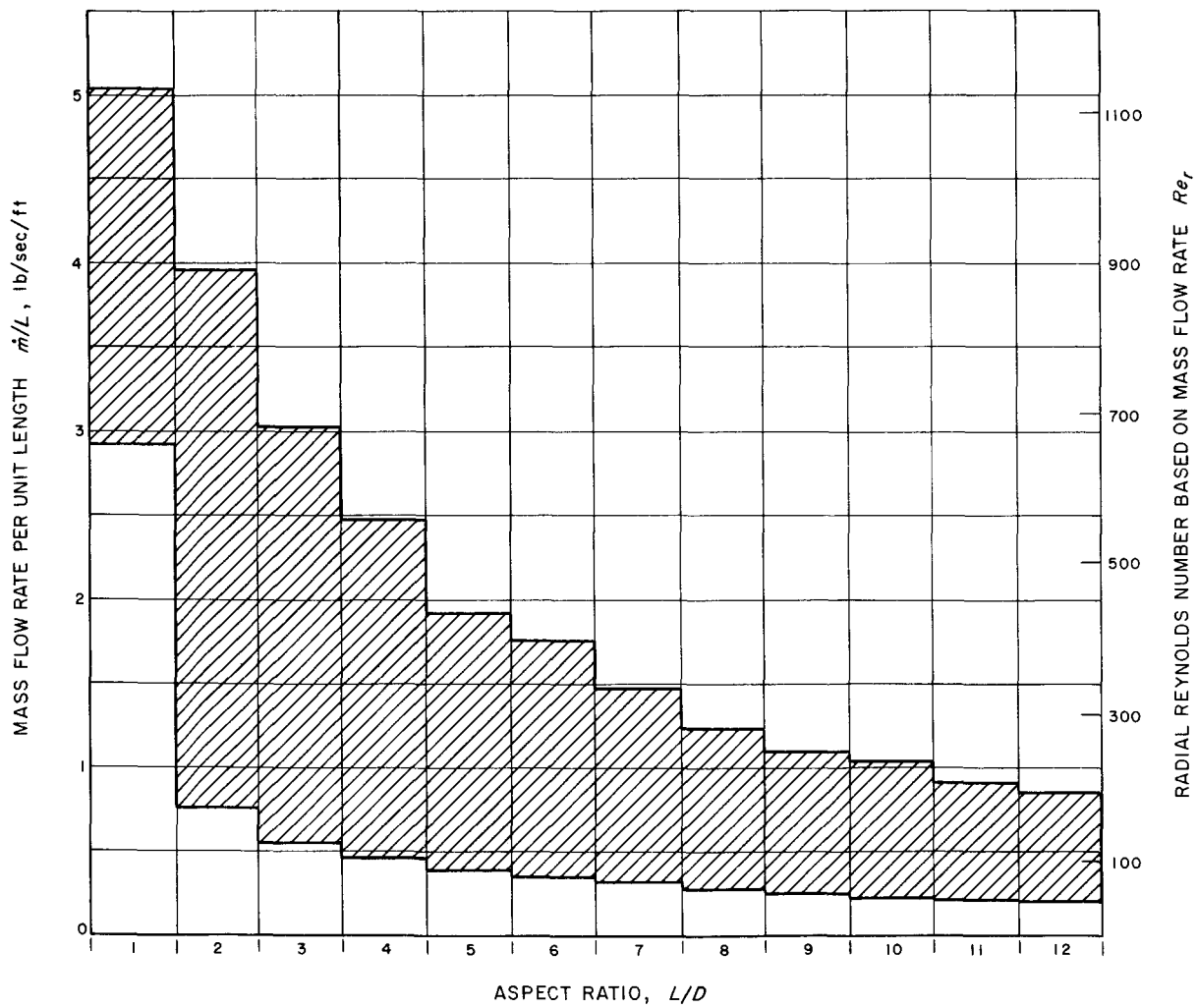

Fig. 5. Range of observation and measurement of end-wall static pressure distribution

particles and, of course, did not affect gas in solution. At times the water either contained such quantities of dirt, or was so highly charged with dissolved gas, that flow visualization studies were hampered. Dirt inclusion should not affect pressure data unless its percent-by-weight becomes too high. In absence of data to the contrary, the same hypothesis is offered for gas inclusion. In a somewhat different, vertically oriented apparatus (Ref. 25), a large amount of gas released as numerous small bubbles markedly affected the flow. However, the buoyancy released in that case was normal to the centrifugal field, in contrast to the orientation used here. In the present experiment, presence of dirt and dissolved gas in large amounts was mainly a visualization hindrance, since the effect was to limit light penetration, scatter the light, and generally limit the detail that could be perceived. On the other hand, observation of small dirt particles was sometimes instructive.

C. Flow Unsteadiness

Flow unsteadiness in this apparatus arose from two sources: (1) the water supply and (2) the vortex flow itself. Depending on the magnitude, frequency, and duration of the flow perturbations, they could be detected by changes in pressure or mass flow-rate levels, or by observing dye motions. To a degree, the two sources mentioned could be identified separately because disturbances from the water supply affected the vortex flow, whereas disturbances arising from the vortex flow were often observed when no change in the water supply occurred. Disturbances in the water supply were delayed sufficiently in arriving at the vortex to determine this visually.

Normal line-pressure available at the test site averaged 92 psig, with fluctuations of about ± 5 psi. First-stage regulation at 50 psig was followed by second-stage regulation operating between 35 and 0 psig. Second-stage regulation was effective in maintaining downstream pressure fluctuations to within ± 0.2 psi, often considerably less. Occasionally, large and rather sudden excursions (approx. 20 psi) in line pressure occurred. Although these departures were quickly corrected by the pressure regulators, the mass flow rate during these non-typical periods changed as much as 10%, producing marked changes in the vortex flow.

Disturbances stemming from the vortex flow were not easy to identify as such. They are so labelled only because they occurred in no direct relation to line-pressure disturbances. Their presence was detected by variations in p_{wc} and occasionally by audible vibrations, which took the form of loud, buzzing sounds. Many of these effects could be reproduced on different days by repeating the experimental conditions under which they occurred; however, not all were reproducible. Generally, the onset of buzzing sounds was accompanied by a jump in p_{wc} of 1 or 2 psi. Flow visualization on these occasions revealed nothing obviously different about the secondary flow structure. Vibration was sometimes sufficient to shake the entire test stand.

Another interesting feature of the vortex flow was that certain combinations of configuration and flow could not be achieved or maintained. Attempts to approach certain conditions apparently resulted in instability that caused transition from one type of flow to another. For example, the vortex would not operate with the nominal 1-in.-diameter exit hole at $L/D = 1$ and $p_{wc} - p_a = 5$ psig. Approaching $p_{wc} - p_a = 5$ from below resulted in a sudden onset of buzzing and an equally sudden jump in wall pressure to 7 or 8 psig. A sufficient increase in mass flow rate would result in cessation of the buzzing. Attempts to approach the 5 psig wall-pressure condition from above were equally unsuccessful. This phenomenon was reproducible for the example given and for several other combinations of run conditions. It is possible that annular hydraulic jump in the exit tube was associated with such performance.

D. Air Core Formation

Air or gas core formation in the vortex was found to be caused by gas coming out of solution with the water, rapid migration to the core, and steady-state discharge into the exit tube. This was demonstrated by arranging an experiment such that the air core for a given situation was continually removed by a vacuum pump connected to the center pressure tap in the closed end-wall. A moisture trap was placed in the vacuum line. This arrangement permitted the removal of all but a barely visible trace of air core in the vortex. In repeated trials all visible air was removed. Closure of a valve in the vacuum line immediately produced an air-core renewal. Air did not re-enter the vortex from the discharge system; instead, it accumulated first at the closed end-wall, forming a new core that grew rapidly in both diameter and length. Transient growth of the new air core was initially very rapid but then proceeded more slowly, so that steady-state was not achieved for several minutes. On certain days, apparently when the supply water was highly charged with gas, minute gas bubbles were seen to form, already far distant from the air core, subsequently to be swept toward the centerline. This process began at a relatively distinct radial location, probably in

a zone of high shear stress, and gave the appearance of a steady-state gray-white cloud. Steady-state appearance, however, was due only to a continual formation–depletion process. These clouds were very effective in scattering incident light.

In general, air cores formed within the vortex had a smooth, glassy surface, much like a small, glass rod placed at the vortex centerline, except in the vicinity of the closed end-wall. There, the air core terminated in a button-shaped tip of larger diameter than itself and the surface had a frothy appearance which disappeared several inches from the end wall. The tips of small air cores, perhaps up to ¼-in. diameter, did not appear to touch the end wall, except in a fleeting, dancing fashion. Air cores of approximately ⅜-in. diameter, and larger, definitely impinged on the end wall, since dry, circular spots then appeared at the center of the end wall. End-wall pressure taps located within the bounds of the gaseous region all gave the same reading, a result partly due to the insensitivity of the pressure gage. Small, liquid droplets adhering to the end-wall surface within the gaseous region were not observed to move radially inward or outward, but rather to move slowly in closed, circular orbits. Thus, it is surmised that the air cores were in solid-body rotation.

Due to the presence of two phases near the vortex center, great care was taken in making end-wall pressure measurements in that vicinity to ensure that pressure leads contained either bubble-free water or droplet-free gas. (Transparent pressure leads were installed for this purpose.)

Readings could not be reproduced unless proper procedure was followed. The centerline pressure reading, in particular, caused some difficulty. The following procedure was adopted as the only satisfactory way of obtaining repeatable readings. Prior to a reading, the pressure lead and gage were carefully purged of gas by means of a water flush. Communication with the end-wall pressure tap was initiated and the pressure gage began to read negatively, or vacuum. The minimum gage reading usually occurred at first appearance of small gas bubbles entering into the pressure lead. This reading was taken as the true steady-state value. Admission of more gas bubbles into the line, and subsequent coalescence to larger size bubbles, resulted in a pressure rise. Due to the smallness and length of the pressure lead (approx. 0.040 in. ID by 3- to 4-ft long), this particular reading consumed a considerable time, varying according to the degree of vacuum present. Readings of 8-psi vacuum or lower generally required at least 2 min to achieve steady state. The technique just described permitted a reading reproducibility of ± 0.2 psi at worst, perhaps ± 0.1 psi average. Pressure fluctuations in the vortex were not, of course, detected on this steady-state, center-pressure reading.

In another way, however, the presence of air cores was a decided advantage, as departures from axisymmetric flow were readily detected merely by sighting down the length of the air core and observing its straightness. This technique proved very effective and was used as standard practice. Skewed air cores were a common occurrence and could be produced by a wide variety of conditions, and seemed to occur with great regularity when using odd, rather than even values of L/D with the nominal $^{9}/_{16}$-in.-diameter exit hole. Most of the data taken on the second largest exit-hole, of nominal ⅞-in. diameter, was taken under similar conditions, therefore not reported here.

Several features of skewed air cores were noted: (1) they appeared undular rather than spiral-shaped, taking the form of a sine wave of low amplitude but long wave length, (2) spatial position was not observed to change with rotation of the piston, (3) spatial position was sometimes markedly affected by movement of the flexible hose attached to the exit tube, (4) off-center movement of the terminal tip, immediately adjacent to the end wall, was detected; the center pressure reading was no longer the lowest, (5) their total amplitudes, in some cases, exceeded 0.1 in., (6) they remained stationary, not rotating with time, in the sense of a crankshaft.

E. Injection System

As illustrated in Fig. 1, the driving-jet orifices were not drilled tangentially to the internal vortex surface but instead to a circle 0.92 of the vortex tube ID. This arbitrary choice was made in the hope that less momentum would be lost in wall shear. Figure 6 shows three types of patterns that occurred when dye, injected through a single orifice several inches from the closed end-wall, was observed through that end wall. When progressing from very low to higher mass flow rates, the jet first appeared attached to the wall, then detached, then straightened, finally impinging on the far surface of the wall. Transition from the first to the second type appeared to be more abrupt than from the second to the third type.

The use of discrete driving jets, of course, gives rise to axial variations in injection velocity. That is, a traverse in the central plane of the jets in the axial direction of

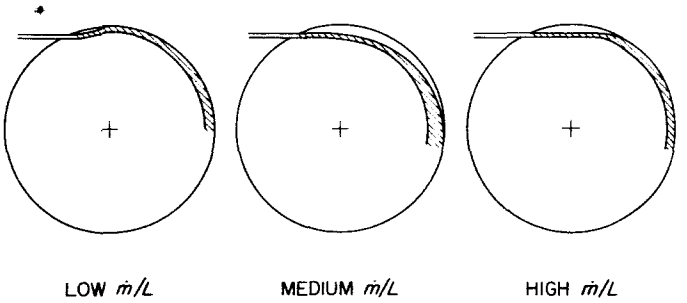

Fig. 6. Approximate appearance of dye injected through a driving-jet orifice, at various rates of flow

the vortex tube would reveal an undular velocity profile: velocity maxima occurring at the jet centerlines and velocity minima occurring half-way between the jet centerlines. The rate of velocity-ripple decay with distance from the jet-orifices (due to mixing and jet-spreading) is of interest. Reference 52 contains analytical and experimental data from which estimates of approach rate toward two-dimensionality may be made. Those results, however, apply to rectilinear jets not immediately influenced by external flow or walls. If the jets are turbulent, it is possible to compute the ripple decay as a function of just two variables: jet spacing ratio (s/d), and non-dimensional distance downstream from the orifice expressed in orifice diameters (x/d). One result is shown (Fig. 7) for a jet-spacing ratio of $s/d = 4$, as employed in this vortex apparatus. The ordinate ϵ represents the difference between the maximum and minimum velocity occurring in the central plane of the jets (i.e., the plane containing the centerlines of the jets, normalized to the maximum velocity). Thus, ϵ represents relative ripple. Figure 7 illustrates that approximately 1% ripple remains 39 orifice diameters downstream of the orifice openings. Applied to the vortex tube directly, this would correspond to a circumferential distance of approximately 2.5 in., or 20% of the peripheral circumference of the vortex tube. The actual distance could be less if reasoned that an applied centrifugal field increases the mixing rate, as results (Ref. 53) plainly indicate.

The effects of injection through discrete holes produces azimuthal variations in tangential velocity as well as axial variations previously discussed. However, the use of slits would not improve this situation. Clearly, an increase in the number of rows of jet-orifices or slits would tend to decrease circumferential variations: a porous wall would be most desirable. Reference 7 contains experimental data and some theoretical estimates of circumferential variations in velocity due to the effect of number of rows. Those results show a rather large effect: the pressure force term $\partial p/\partial \theta$ in the tangential

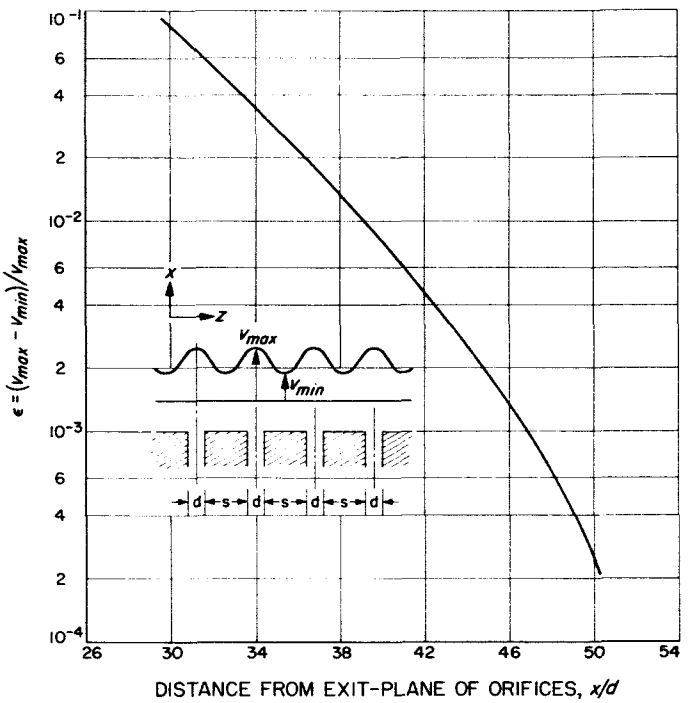

Fig. 7. Decay of velocity defect for turbulent jets issuing from a series of holes in-line, computed for $s/d = 4$, using Eq. (18) of Ref. 52

momentum equation was found to be approximately 70% of the inertial term for one-site injection, 20-25% for two-site injection, but negligibly small for four-site injection.

F. Instrument and Reading Errors

Some indication of instrument error has been given in previous sections. Additional comments and a summary in this connection follow. The accuracy of the bourdon-tube pressure gage, as supplied by the manufacturer, was $\pm 0.25\%$ full-scale reading; individual accuracy of the rotameters under ideal conditions was judged to be $\pm 1.0\%$ or, since three were used, a total of $\pm 3\%$ full scale. These values are irrelevant considering reproducibility in the presence of flow unsteadiness. Stated in absolute terms, accuracy and reproducibility of mass rate of flow readings and static pressure readings were judged to be ± 0.2 lb/sec and ± 0.2 psi, at worst. Readings not within these bounds were either not recorded, recorded with qualification, or delayed until better conditions prevailed.

G. Method of Taking Data

With a given installation of exit-hole and exit-tube size, static pressure surveys at the closed end-wall were

taken for integral values of L/D, each through a range of wall pressure values $5 \leq (p_w - p_a) \leq 35$ psig in 5 psi increments. Mass rate of flow and water temperature were recorded for each condition. This procedure was repeated for each of the five exit-hole sizes employed. Photography of dye motions was not undertaken during this test period; however, dye motions were often observed visually, especially when unusual circumstances were suspected.

Internal probings of the flow were initially planned but attempts to secure this type of data were abandoned for reasons to be discussed later.

H. Dimensional Stability of the Vortex Tube

Inspection of the plexiglas vortex tube before assembly revealed that the actual internal diameter of the finished tube was 3.972 $\pm$0.001 in., both circumferentially and axially. Between $0 < L/D < 1$, as measured from the closed end-wall, a taper of 3.935 to 3.972 occurred. After several months of intermittent running, the apparatus was disassembled and the vortex tube re-inspected. The tube was then found to be somewhat barrel-shaped, measuring 3.944 $\pm$0.001 and 3.975 $\pm$0.001 in. at the ends, and 3.985 $\pm$0.003 in. between the ends. It is doubtful that such small discrepancies had any large effect on the flow, or that they gave rise to unsteadiness in the flow. The vortex tube inspection just referred to also revealed that overall length of the vortex tube had increased by 0.090 in. over its original length of approximately 51 in. Dimensional changes in the vortex tube are thought to be the result of cold flow in the plexiglas material induced by the action of fluid pressure; they cannot be explained on the basis of thermal expansion or water absorption.

IV. EXPERIMENTAL RESULTS

A. Introduction

Certain remarks concerning the nature of the experiment and treatment of the data are appropriately stated as a preface to presentation of data.

It is emphasized that changes in aspect ratio in this apparatus were accomplished by changing its length while holding its diameter fixed. This is an important distinction because the effects of varying aspect ratio are not necessarily, and probably not, independent of vortex scale (e.g., a scale based on vortex diameter). Data will be presented, where appropriate, in terms of L/D rather than absolute vortex length because L/D is more convenient to use and, probably, somewhat easier to imagine. Other obvious ways to vary aspect ratio would be less convenient and difficult to interpret. For example, the diameter of a vortex could be varied while holding its length fixed. Such an experiment would very likely yield results decidedly different than those presented here because the effects of cylindrical-wall friction would vary with vortex diameter. Reference 54 contains discussion relevant to that problem. At present, there are no satisfactory scaling laws for vortex flows.

Because of limited accuracy of data, which is more crucial in some instances than in others, the data is presented in ways intended to establish trends, rather than to portray precision. Outside of necessity, this method of presentation is well attuned to the qualitative nature of flow-visualization. Where possible, comparisons to some of the simple analytical results (Ref. 55) are given.

B. Air Core Size

From experience gained in operating the vortex apparatus, it was quickly determined that the size or diameter of the air core was strongly dependent on aspect ratio and exit-hole size, but not greatly affected by mass rate of flow. However, in the case of the two smallest exit holes (nominally ½-in. and 9/16-in. diameter), the vortex would not sustain an air core at all if $\dot{m}/L$ fell below approximately 0.55 lb/ft/sec. Air-core diameters were estimated visually over the range of operation. These estimates were too inaccurate to delineate pressure or mass rate of flow effects but were adequate to show the effects of aspect ratio and exit-hole size. Increasing L/D, with a given exit-hole size, resulted in

a decreasing air-core diameter. Increasing exit-hole size, at constant L/D, resulted in increasing air-core diameter. The observed variation of air-core diameter with a combined parameter, including both L/D and d_e, is illustrated (Fig. 8). Despite considerable scatter, the data exhibit a recognizable trend.

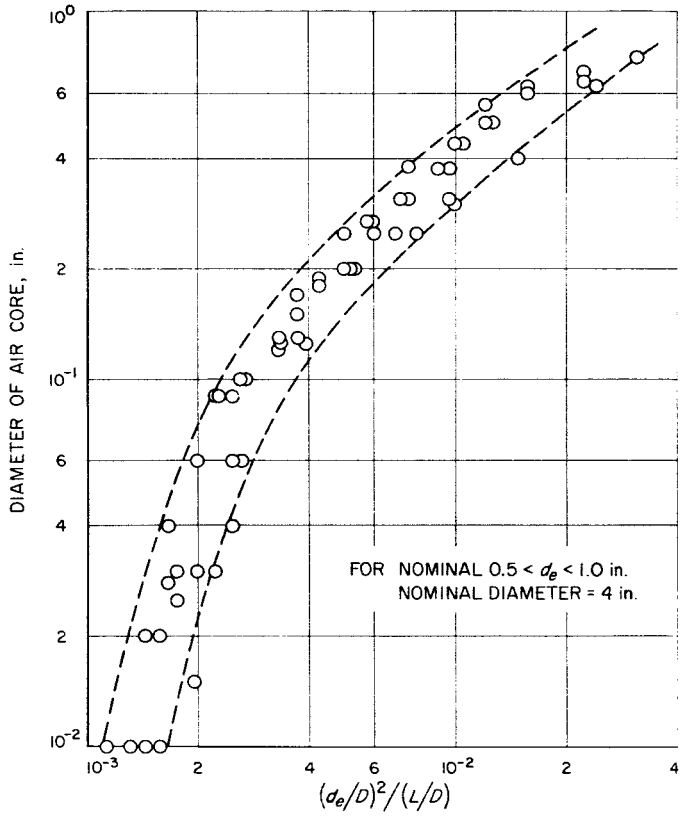

Fig. 8. Approximate observations of air-core diameter correlated with exit-hole size and aspect ratio

The disappearance of the air core, under some conditions, occurred because the rate of bubble removal in the axial direction exceeded the rate of bubble generation and migration toward the axis in the radial direction. Decrease in air-core diameter with increasing L/D is in general agreement with the observation (to be discussed later) that the viscous core of the vortex also tended to decrease in diameter with increasing L/D. The viscous core region of a vortex is not precisely defined, but it is that portion of a real vortex flow which tends to approach solid-body rotation. Vortex core shrinkage could be viewed as a concentration in vorticity brought about by vortex stretching. Another viewpoint might be that an increase in circulation near the vortex axis is caused by increased radial mass flow rate, thus requiring an accommodation in core diameter.

In a later experiment, the apparatus was arranged so the air core within an exit tube could be observed visually. This was done using a nominal 1-inch-diameter exit hole and matching exit tube fabricated from plexiglass. Such observations were prompted by a general desire to learn more concerning structure and shape of an air core in a decaying swirl flow. More particularly, the desire was to learn whether the air core remained intact throughout the exit tube and, if not, to examine the termination of the air core for evidence of unsteadiness. As stated earlier, the possibility had been considered that unsteadiness often observed in the vortex flow was related, in some way, to the flow in the exit tube. Observations revealed that the air core did not persist throughout the exit tube, but terminated within it, at a position varying with flow conditions in the vortex. Prior to termination, the air core possessed a spirally-convoluted, or braided surface, very similar to those observed by Binnie (Ref. 28). The overall diameter decreased with distance downstream. The terminal end was never steady due to a continuous breaking-off of air bubbles of random size which then passed downstream. At higher mass rates of flow, this break-off process appeared to be extremely violent, resulting in significant vibration. However, it was difficult to determine any correlation between these motions and the motion of dye within the vortex. Unfortunately, no pressure taps were located along this exit tube, therefore it is not known whether air-core termination was associated with some form of annular hydraulic jump.

C. *Mass Rate of Flow Measurements*

The mass rate of flow per unit length is plotted (Fig. 9) as a function of pressure drop across the driving-jet orifices. The experimental data cover a wide range of variations in aspect ratio and exit-hole size. From this data, it can be at once concluded the driving-jets themselves were turbulent [since $\dot{m}/L \propto (\Delta p_j)^{0.55}$], indicating that the flow in the driving-jet orifices was very near a state of fully-developed turbulent flow. According to Ref. 56, two-dimensional jets remain laminar up to jet Reynolds numbers of approximately 30, where the jet Reynolds number is based on slit diameter and efflux velocity. This value is far below the lowest values occurring in these experiments. A plot, similar to Fig. 9, is given in Ref. 29 for the case of water flow in a toroidal vortex. In the latter case, it was determined that $\dot{m}/L \propto (\Delta p_j)^{0.62}$.

The variation of $\dot{m}/L$ with static pressure at the cylindrical wall is shown (Fig. 10) for each of the five

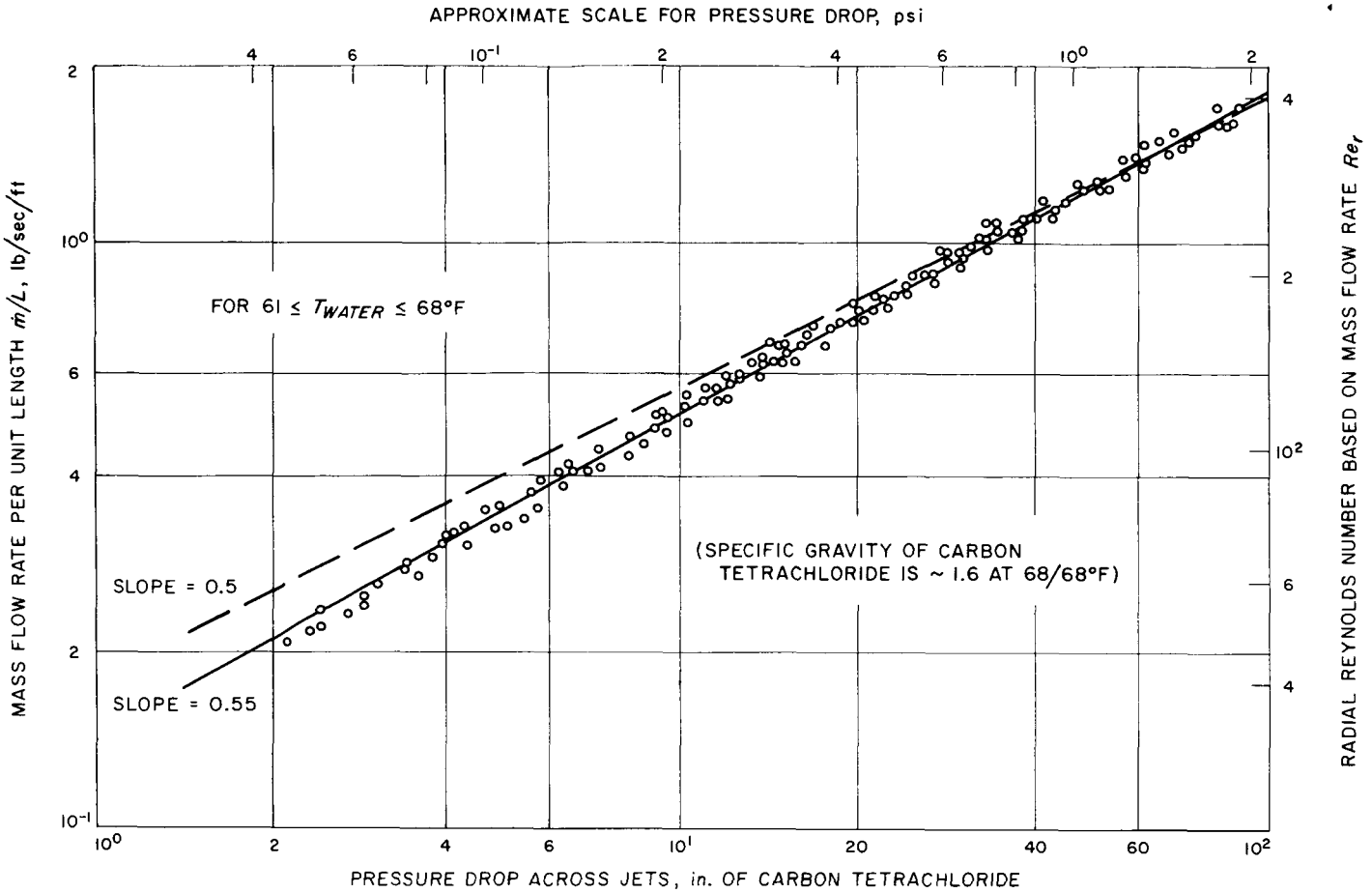

Fig. 9. Mass flow rate per unit length $\dot{m}/L$ as a function of pressure drop across the driving-jet orifices

exit holes. Since the vortex discharged to atmospheric pressure through the exit tube, the gage pressure given as $p_w - p_a$ merely represents the overall pressure drop across the vortex and exit-tube system. Except for the two largest exit holes, the slopes of the lines (Fig. 10) are approximately 0.5. This result is not necessarily indicative of turbulent flow through the vortex, since the same result would be obtained if the flow process were merely frictionless accelerated flow through a restriction. However, any comparison of a confined vortex flow to a simple, hydraulic resistance element should be made cautiously. For example, this apparatus would consist of at least four resistive elements in series: (1) the driving-jet orifice friction, (2) cylindrical wall-friction, (3) a parallel network of end-wall friction and internal fluid friction within the vortex, (4) exit-tube friction. Of the four, which are interrelated in complex ways, only (1) was well determined in this experiment.

Deviations or discontinuities in the curves (Fig. 10) are evident for the three largest exit holes at low values of L/D. The reasons for these deviations are not known; possibly they represent transition from one type of flow to another.

A crossplot shows the effect of L/D on $\dot{m}/L$ for the three smallest exit holes (Fig. 11). These curves also exhibit departures from straight-line relations that are either small discontinuities or, more probably, changes of slope. However, the effect of L/D is indicated in wide approximation by $\dot{m}/L \propto (L/D)^{-3/4}$. The fact that $\dot{m}/L$ increases as L/D decreases at constant p_w indicates that less total frictional resistance is encountered at low L/D because the total mass rate of flow $\dot{m}$ is lower and the fluid path length decreases. Thus, the axial pressure drop in some region of the vortex core must increase with increasing L/D to maintain a fixed $\dot{m}/L$. In the latter case, an increase in wall pressure is also required (Fig. 12).

An attempt to coalesce the data (Fig. 10) into one curve is shown (Fig. 13) for the three smallest exit holes;

data for the nominal $11/16$-in.-diameter exit hole at $L/D = 2$ has been omitted from this plot. Data points for the two largest exit holes do not fall on the curve, but usually lie above it. The abscissa (Fig. 13) is not dimensionless but could be rendered so, merely by normalizing to some reference pressure. The use of this

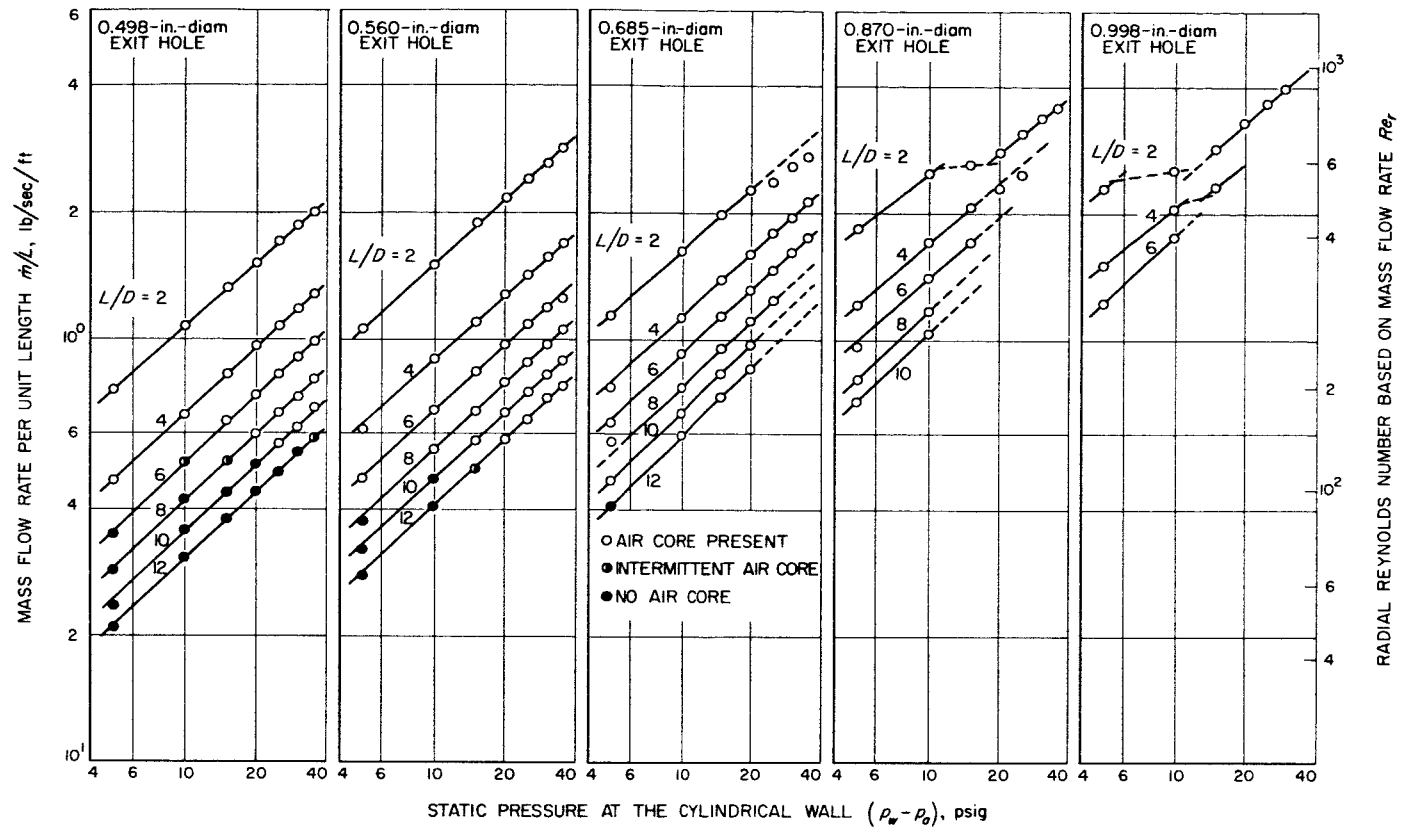

Fig. 10. Variation of mass flow rate per unit length with static pressure at the cylinder wall, aspect ratio as parameter

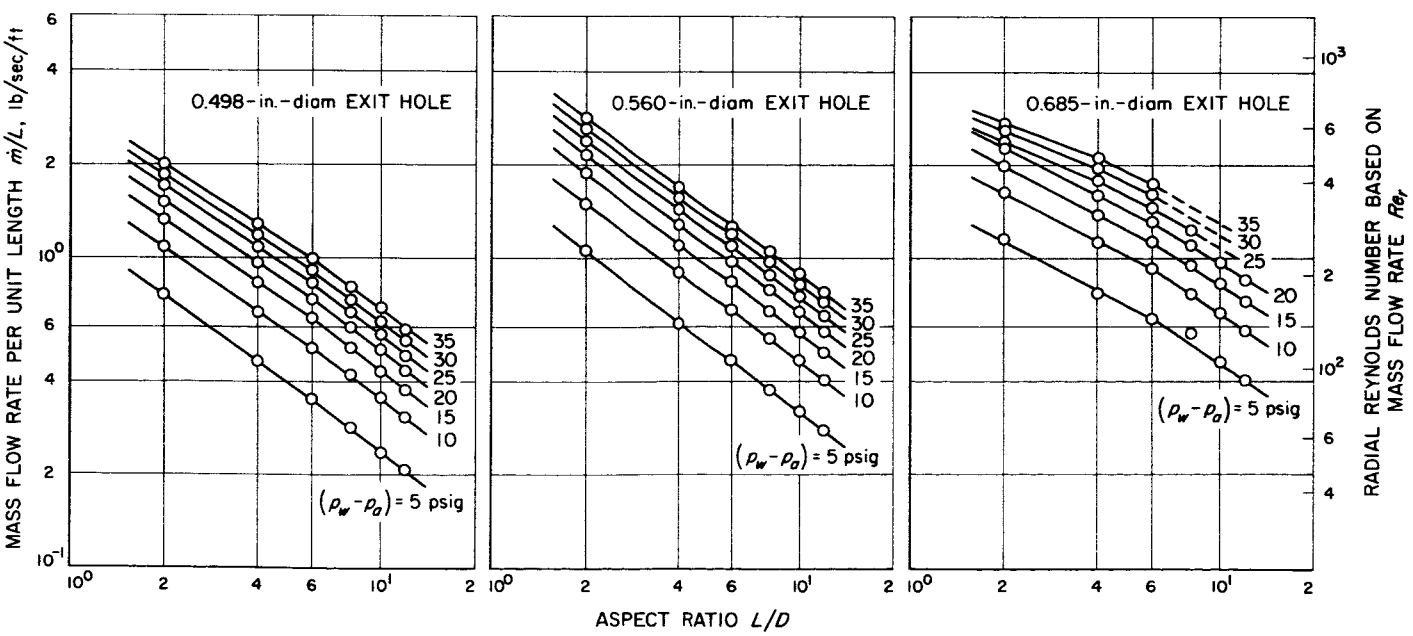

Fig. 11. Variation of mass flow rate per unit length with aspect ratio, static pressure at cylindrical wall as parameter

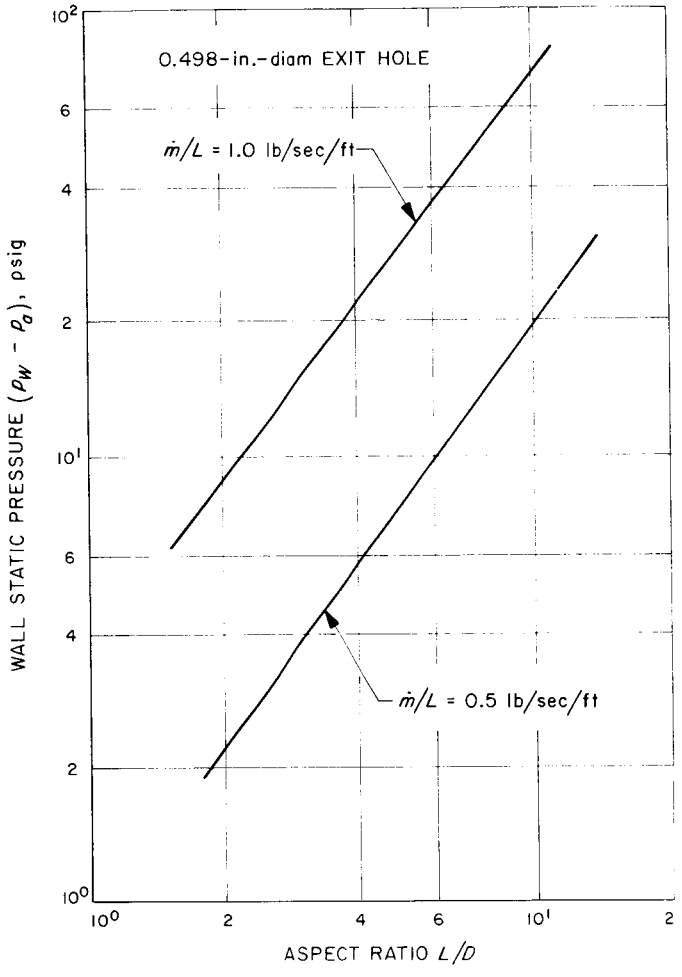

Fig. 12. Wall static pressure requirements to maintain constant mass flow rate per unit length at varying aspect ratio

parameter is somewhat misleading in that the conclusion might be drawn that $\dot{m}/L \propto (D)^{-1.25}$; this would be an erroneous conclusion since the effects of D were not investigated at all. A clearer statement would read as follows: For these three exit holes, it was determined that $\dot{m}/L$ increases directly as $(p_w - p_a)^{1/2}$, increases directly as the area of the exit hole or d_e^2, and decreases inversely as $L^{3/4}$.

D. Static Pressure Measurements

Static pressure was measured at 16 radial stations on the closed end-wall and at 4-in. intervals axially (but not circumferentially) along the cylindrical wall of the vortex tube. Five of the eight end-wall taps in interval $0.35 \leq r/r_w < 1.0$ were discarded because pressure differences between these taps were normally very small and, using a pressure gage, could not be measured with precision. Preliminary measurements were obtained over a wide variety of test conditions, using the axially-distributed set of taps. These measurements (using a manometer bank) indicated no significant axial pressure gradients existed along the cylindrical wall and were discontinued. Pressure at the cylindrical wall for all successive tests was measured at axial position $L/D = 1$ from the closed end-wall. Pressure, within or internal to the vortex and/or along exit-tube wall, was not measured.

Although end-wall pressure taps were installed as closely together as could be managed near the vortex centerline, this distribution proved to be too coarse. As a result, end-wall static pressure distributions were not well determined in interval $0 < r/r_w < 0.05$. This is unfortunate because the largest radial pressure gradients often occurred in that region.

The static pressure distributions for three of the five exit holes are shown (Figs. 14, 15, and 16) for various values of wall pressure p_w and aspect ratio L/D. Changes in p_w are comparable to changes in $\dot{m}/L$. The effects of exit-hole size and mass rate of flow are not unusual (Ref. 11). In comparison with gas vortex results (Ref. 11), the water vortex has a flatter, broader pressure distribution in the annular portion of the vortex, but a narrower, steeper distribution in the core region. It is seen (Figs. 14, 15, and 16) the principal effect of an increase in L/D is to reduce effective size of the vortex core, thereby causing a steeper pressure distribution in that region. Broadly speaking, the effect of an increase in L/D on pressure distribution is similar to the effect of reducing exit-hole size with constant L/D. Flat pressure distribution observed in the core region, when using the largest exit hole (Fig. 16), is due to existence of a large air core. The air core, in that case, was probably in solid body rotation, producing pressure gradients too small to be detected by the pressure gage.

A comparison of pressure distributions obtained at constant p_w, but varying L/D, is illustrated (Fig. 17) for the three smallest exit holes. Again, an effect of L/D is to decrease core size, but now, with constant p_w, crossovers occur in the core region because of center-pressure variations. It is difficult to determine what value of L/D yields maximum pressure gradient from data presented (Fig. 17) because normalized pressure p/p_w has been plotted. The maximum radial pressure gradient does not appear to have been reached, even at $L/D = 12$, in any of the three cases.

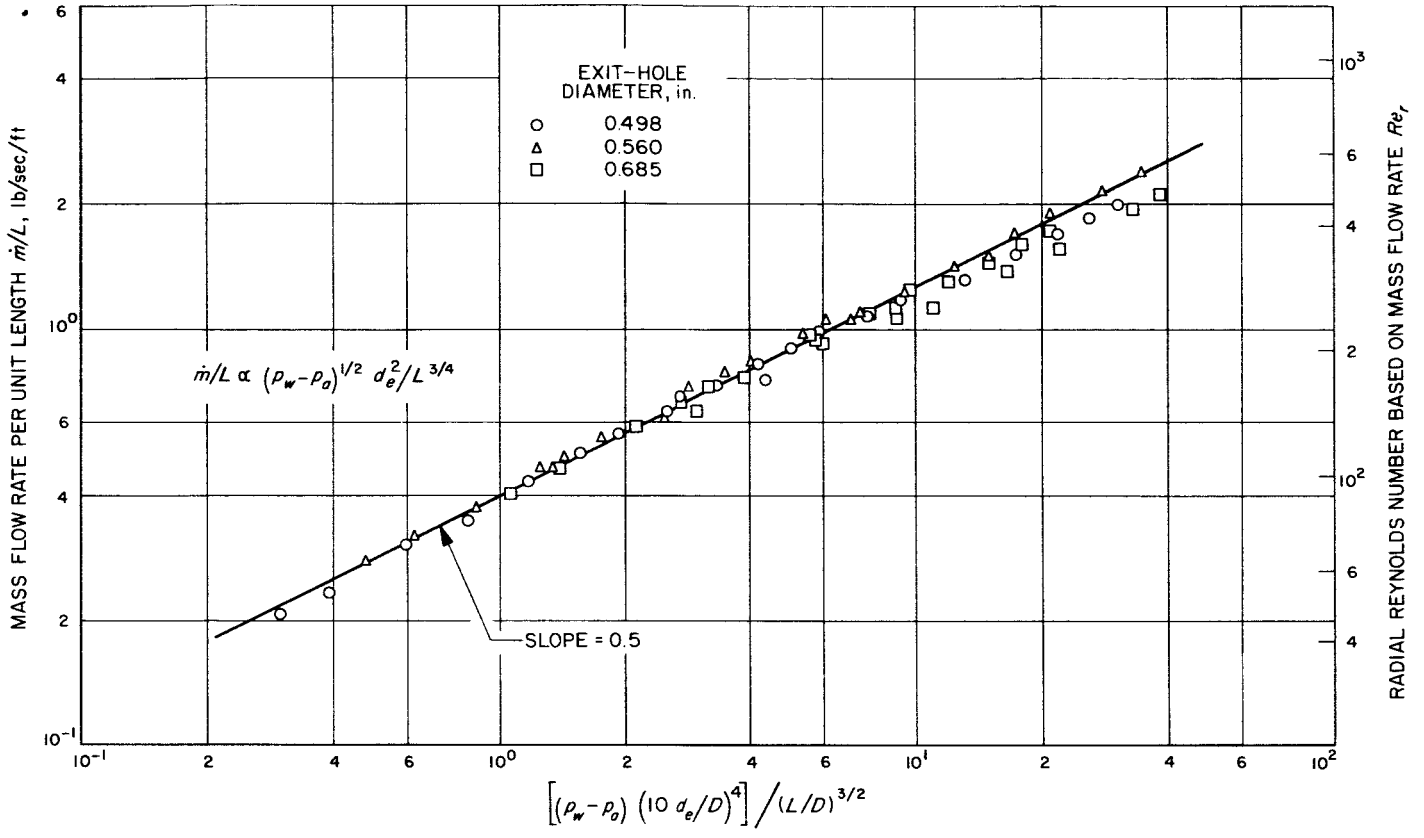

Fig. 13. Correlation of mass rate of flow per unit length with static pressure at cylindrical wall, exit-hole diameter, and vortex length

The results shown (Fig. 17) may be compared with those of Fig. 5, Ref. 11, which refer to variations of $0.78 < L/D < 2.5$ at constant p_{ic} in a gas vortex. The two cases differ, in that the gas vortex exhibits an increasingly depressed pressure distribution as L/D increases, whereas the water vortex has distribution levels that increase with increasing L/D, except near the vortex axis, where crossovers occur. The comparison is poor, however, because the L/D range covered by the two experiments is entirely different. A series of pressure distributions is shown for various exit-hole sizes at constant L/D and approximately constant p_{ic} in Fig. 6 of Ref. 11. That series of distributions is remarkably similar to the set shown for the largest of the three exit holes (Fig. 17).

Another method of presenting and comparing pressure distributions is shown again for the three smallest exit holes (Fig. 18). In this case, the total mass rate of flow $\dot{m}$ has been held approximately constant, while L/D has been allowed to vary. Each set of curves shows an orderly progression without crossovers. Differences in pressure distributions for a given exit hole are not confined to the core region, but rather span the whole radial extent of the vortex. The effect of holding $\dot{m}$ constant while increasing L/D is to produce vortexes of successively lower strength. An analogous theoretical case (Ref. 55) for a two-dimensional vortex flow indicated that the effective radial Reynolds number for constant $\dot{m}$ first increases sharply, attains a maximum value, and then decreases gradually as L/D increases. The experimental case, as judged by the radial gradient of pressure, does not appear to follow this trend, insofar as yielding an optimum L/D. The experimental and theoretical cases are not directly comparable, however; the theoretical model yields information only on the effective radial Reynolds number and has not been extended to predictions of radial pressure or tangential velocity distributions. Variation of p/p_{ic} with L/D is shown at several radial stations (Fig. 19). A general rise in p/p_{ic} occurs with increasing L/D at any radial station. Variations with increasing L/D are clearly not confined to the core region.

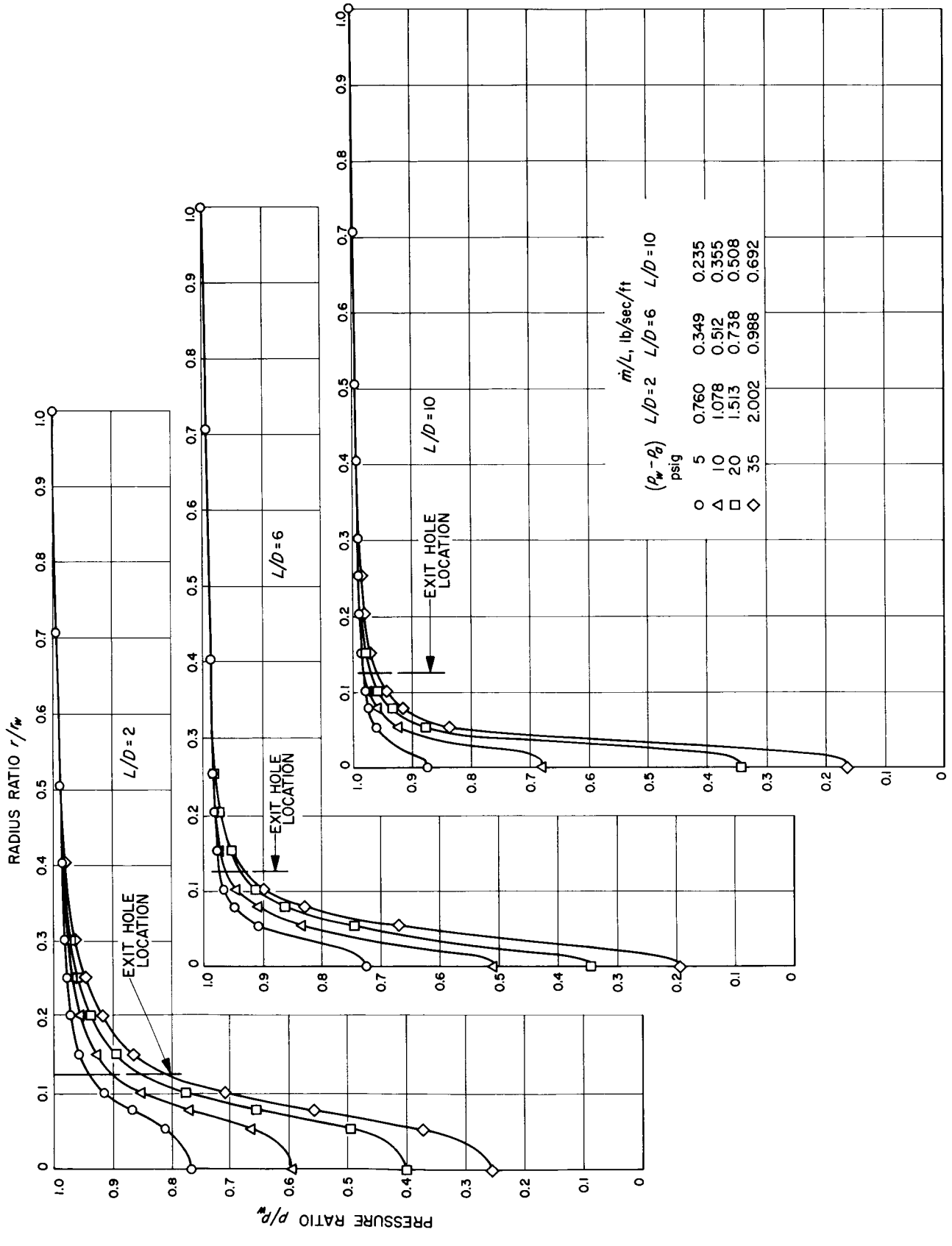

Fig. 14. Radial pressure distributions at closed end-wall for 0.498-in.-diam exit hole

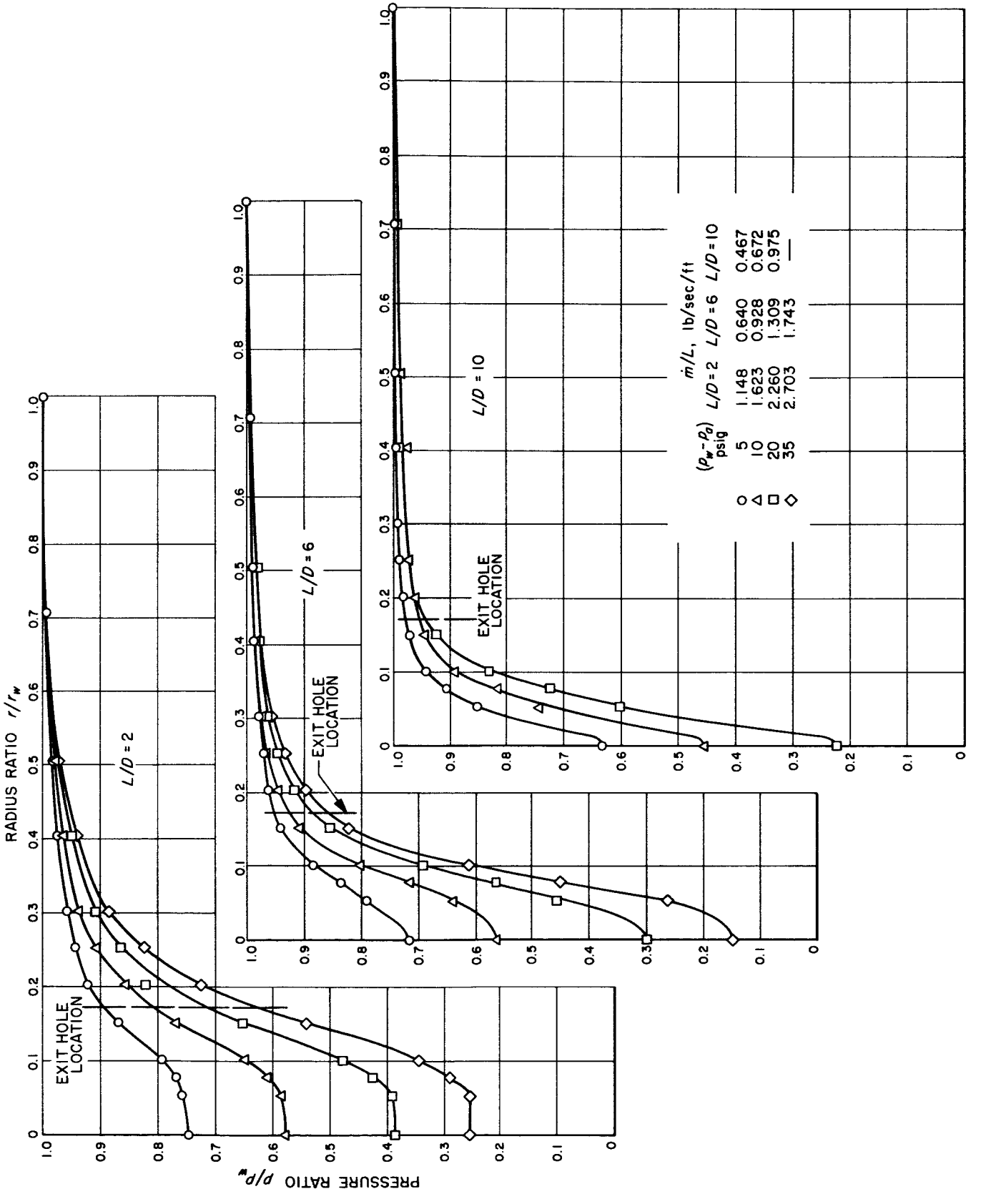

Fig. 15. Radial pressure distributions at closed end-wall for 0.685-in.-diam exit hole

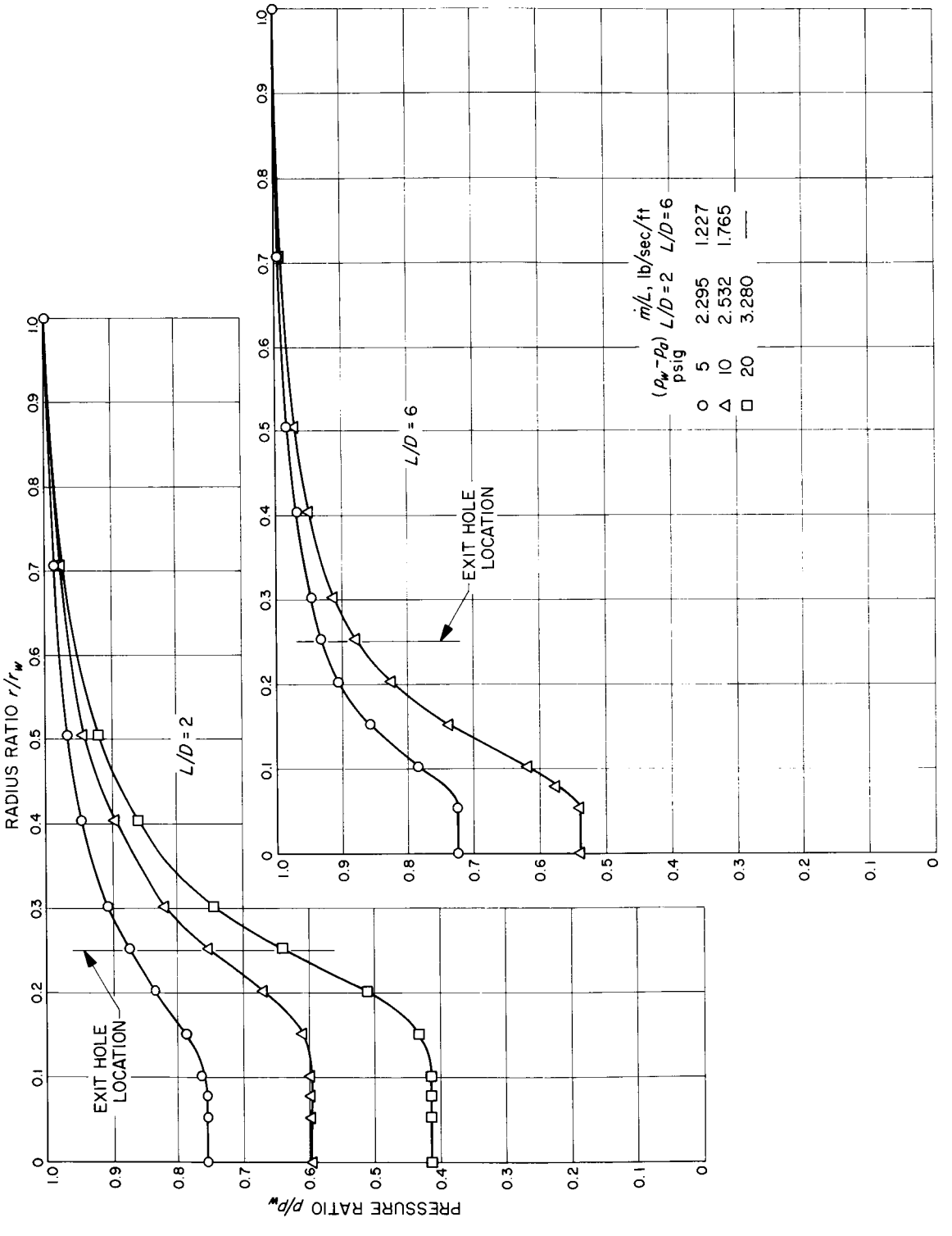

Fig. 16. Radial pressure distributions at closed end-wall for 0.998-in.-diam exit hole

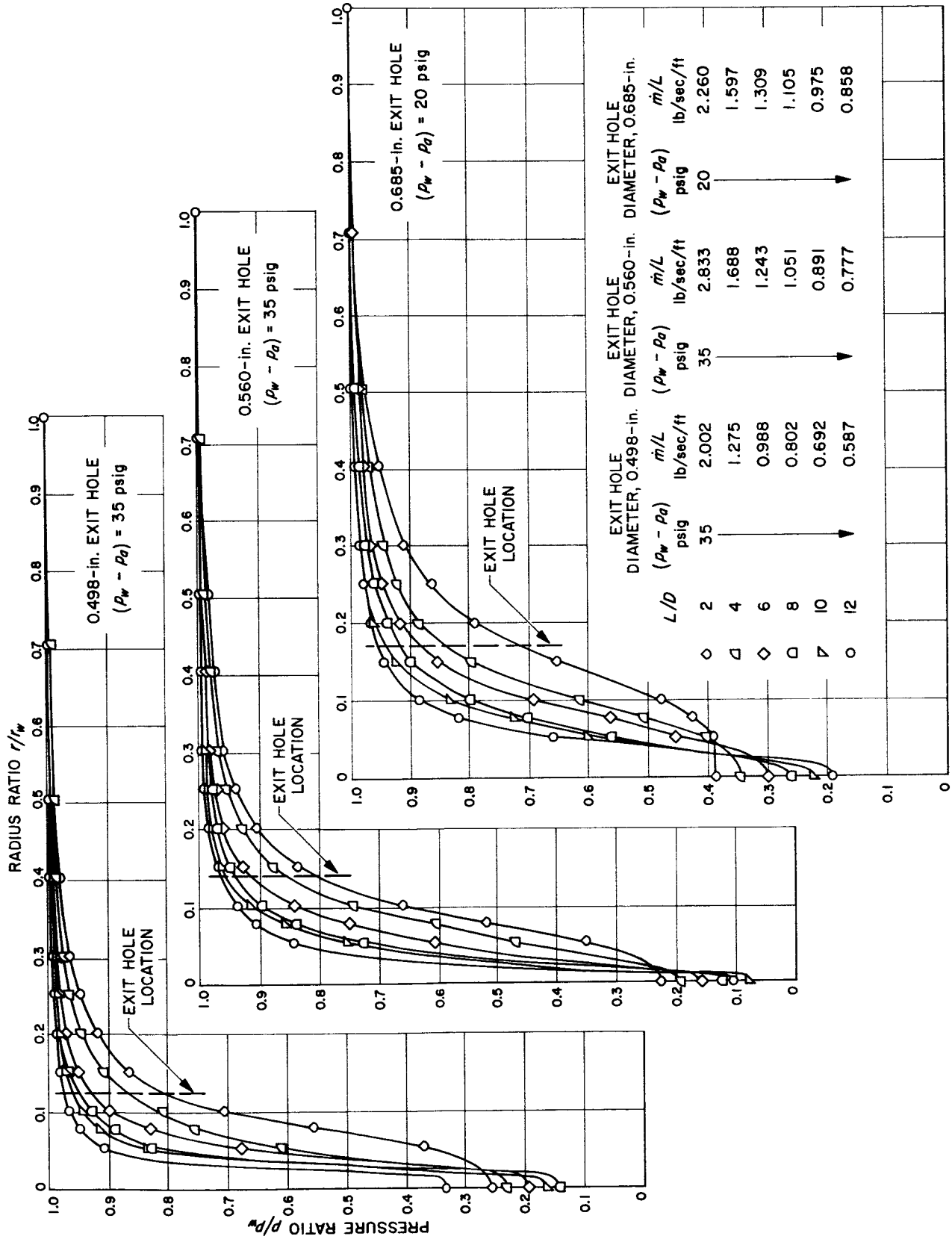

Fig. 17. Radial pressure distributions at closed end-wall—variation with aspect ratio at constant static wall pressure

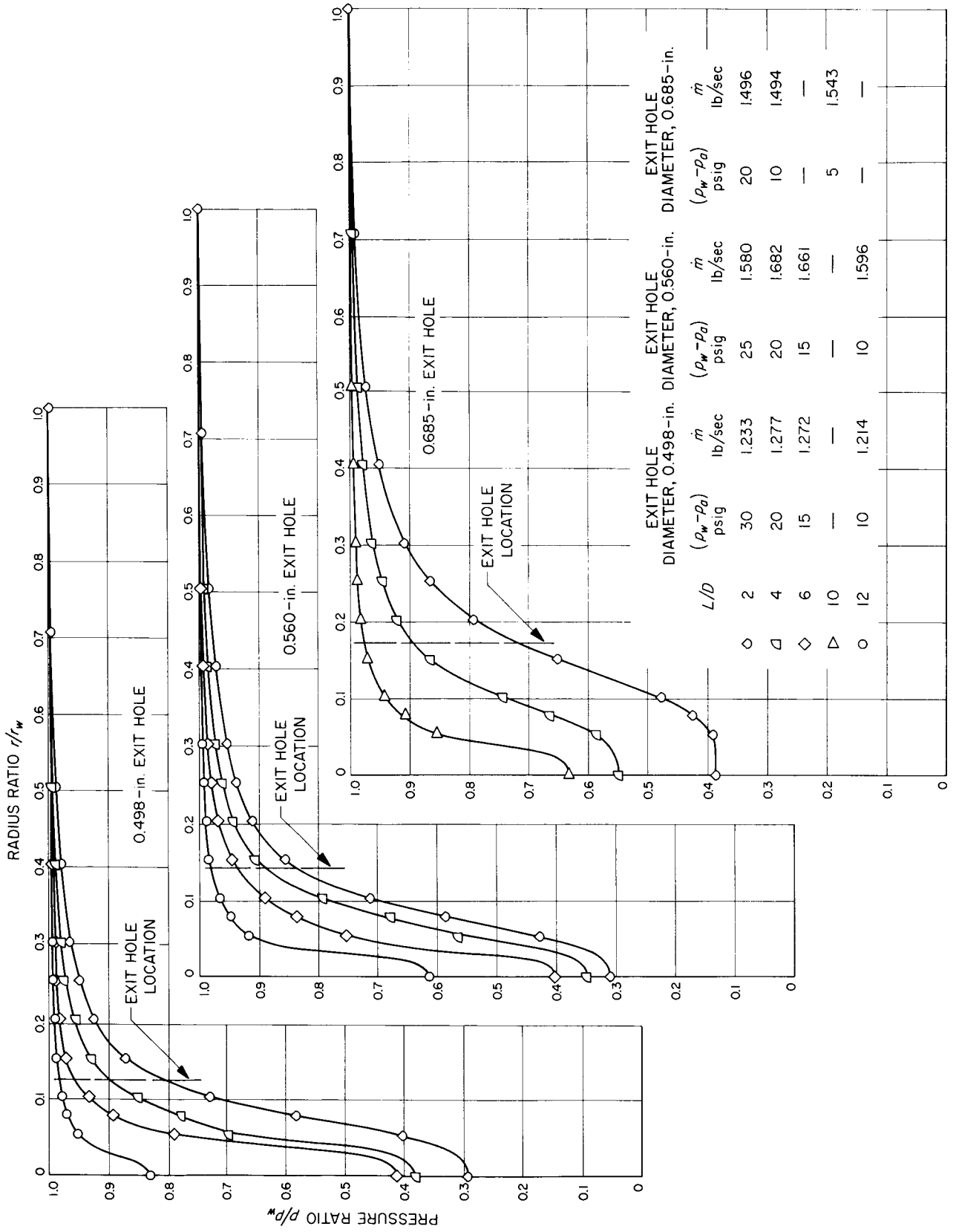

Fig. 18. Radial pressure distributions at closed end-wall—variation with aspect ratio at approximately constant total mass flow rate

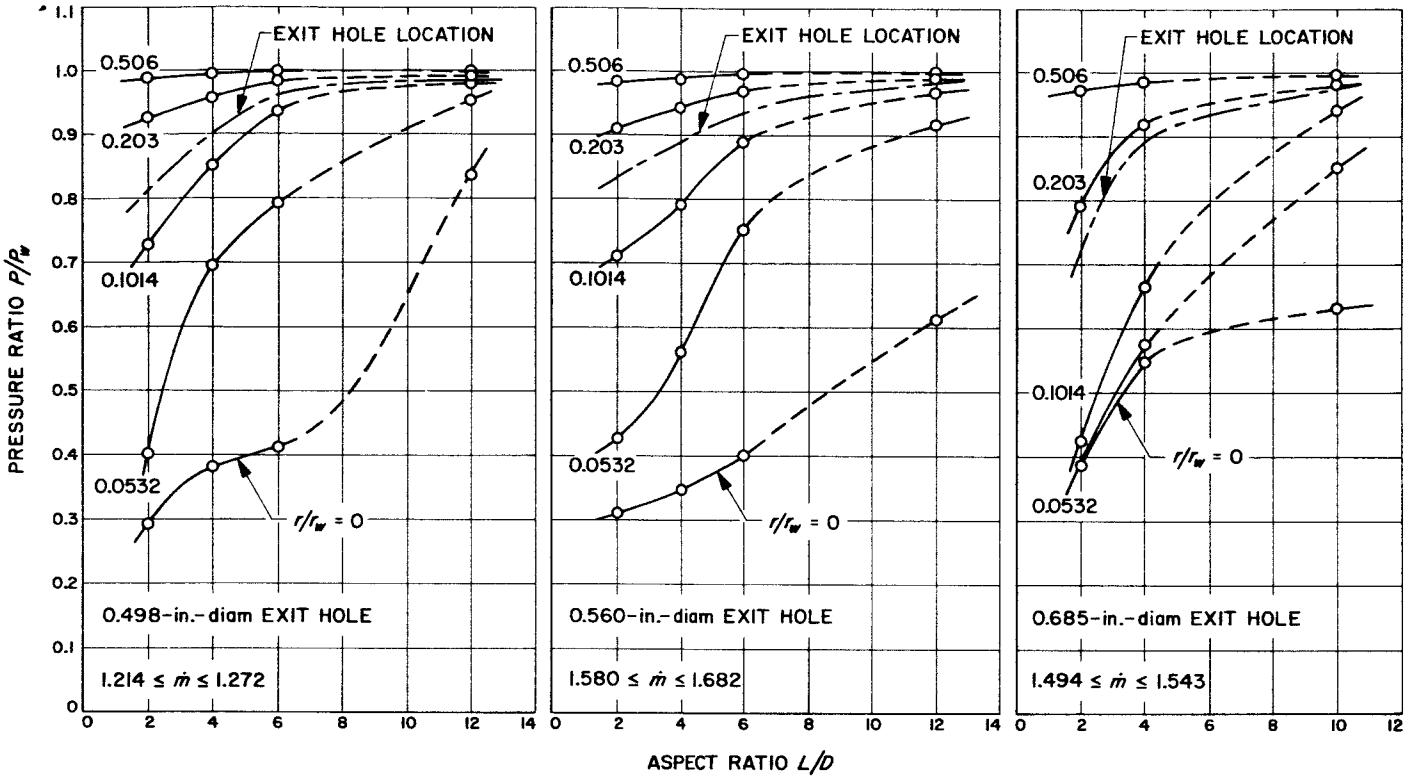

Fig. 19. Static pressure at various radial stations—variation with aspect ratio at approximately constant total mass flow rate

According to the two-dimensional vortex solution (Einstein and Li, Ref. 14), tangential velocity and static pressure are functions of radius only (neglecting gravitational head). The only independent flow parameter is the radial Reynolds number, which is directly proportional to $\dot{m}/L$. Increasing Re_r or $\dot{m}/L$, while holding a fixed exit-hole size, results in increasing vortex strength, such that peak value of v/v_w increases monotonically with $\dot{m}/L$. This solution is independent of L/D. Hence, studying effects of varing L/D, while holding fixed $\dot{m}/L$, should give a meaningful comparison between theory and experiment. In Ref. 55, the effect of radial mass-flow depletion, due to diversion of flow into the end-wall boundary layers, has been cast into an effective radial Reynolds where $Re_{r,e} \ll Re_r$. It was subsequently shown that $Re_{r,e}$ increased monotonically with L/D, while holding $\dot{m}/L$ fixed; further, that $Re_{r,e} \rightarrow Re_r$ as $L/D \rightarrow \infty$ (i.e., the end-wall boundary layers) became progressively less influential as L/D became increasingly large. This two-dimensional model cannot be realistic, since axial pressure gradients were entirely neglected; however, it is a convenient model easily applied.

The analogous experimental case for the water vortex is presented in Figs. 20 and 21, in which pressure distributions for varying L/D, with approximately constant $\dot{m}/L$, are shown for the three smaller exit holes. Comparison between Figs. 18 and 20 shows a striking difference. For a given exit-hole size, Fig. 20 shows that differences in pressure distributions with varying L/D are largely confined to the core region when $\dot{m}/L$ is constant. This is not the case when $\dot{m}$ is held constant (Fig. 18). Figures 19 and 21 bring out this contrast even more clearly; moreover, the variation of p/p_w, with L/D in the core region, is entirely different for the two cases.

Turning attention again to Fig. 20, it appears that the maximum radial pressure gradient increases with increasing L/D and has not yet reached an optimum in the interval $0 \leq L/D \leq 12$. If this were true, then v/v_w also increases with increasing L/D, which is in agreement with the prediction of Ref. 55. The agreement may be fortuitous, but, in any case, it is in trend, not magnitude. The experiments, being limited to $L/D \leq 12$, are not a very convincing test of the theory. It is not likely that further increases in L/D would have produced significantly greater radial pressure gradients than those obtained.

Few closed-form solutions for static pressure in vortex flows have been developed because of difficulties involved

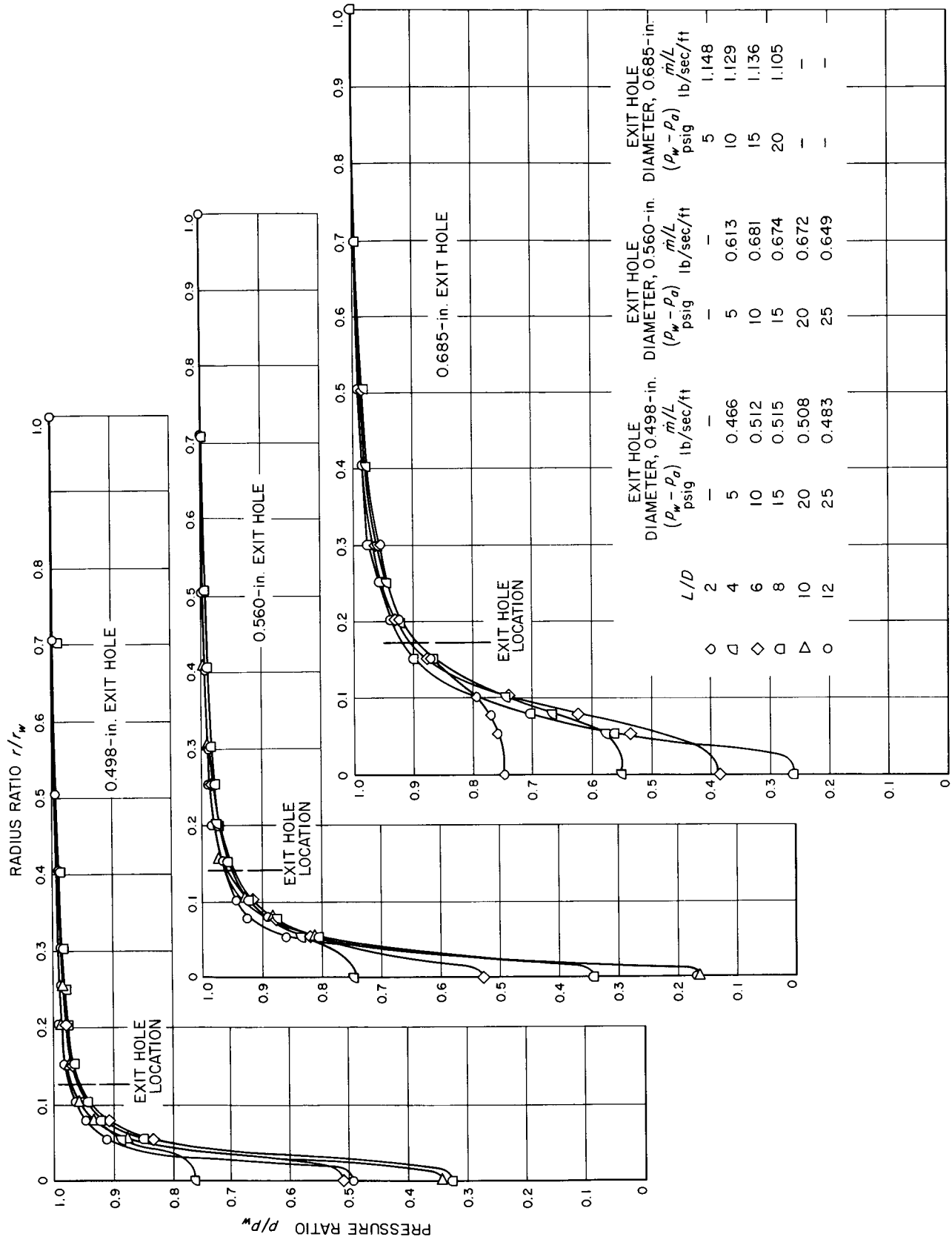

L/D	0.498-in. $(p_w - p_a)$ psig	0.498-in. $\dot{m}/L$ lb/sec/ft	0.560-in. $(p_w - p_a)$ psig	0.560-in. $\dot{m}/L$ lb/sec/ft	0.685-in. $(p_w - p_a)$ psig	0.685-in. $\dot{m}/L$ lb/sec/ft
2	—	—	—	—	5	1.148
4	5	0.466	5	0.613	10	1.129
6	10	0.512	10	0.681	15	1.136
8	15	0.515	15	0.674	20	1.105
10	20	0.508	20	0.672	—	—
12	25	0.483	25	0.649	—	—

Fig. 20. Radial pressure distributions at closed end-wall—variation with aspect ratio at approximately constant mass flow rate per unit length

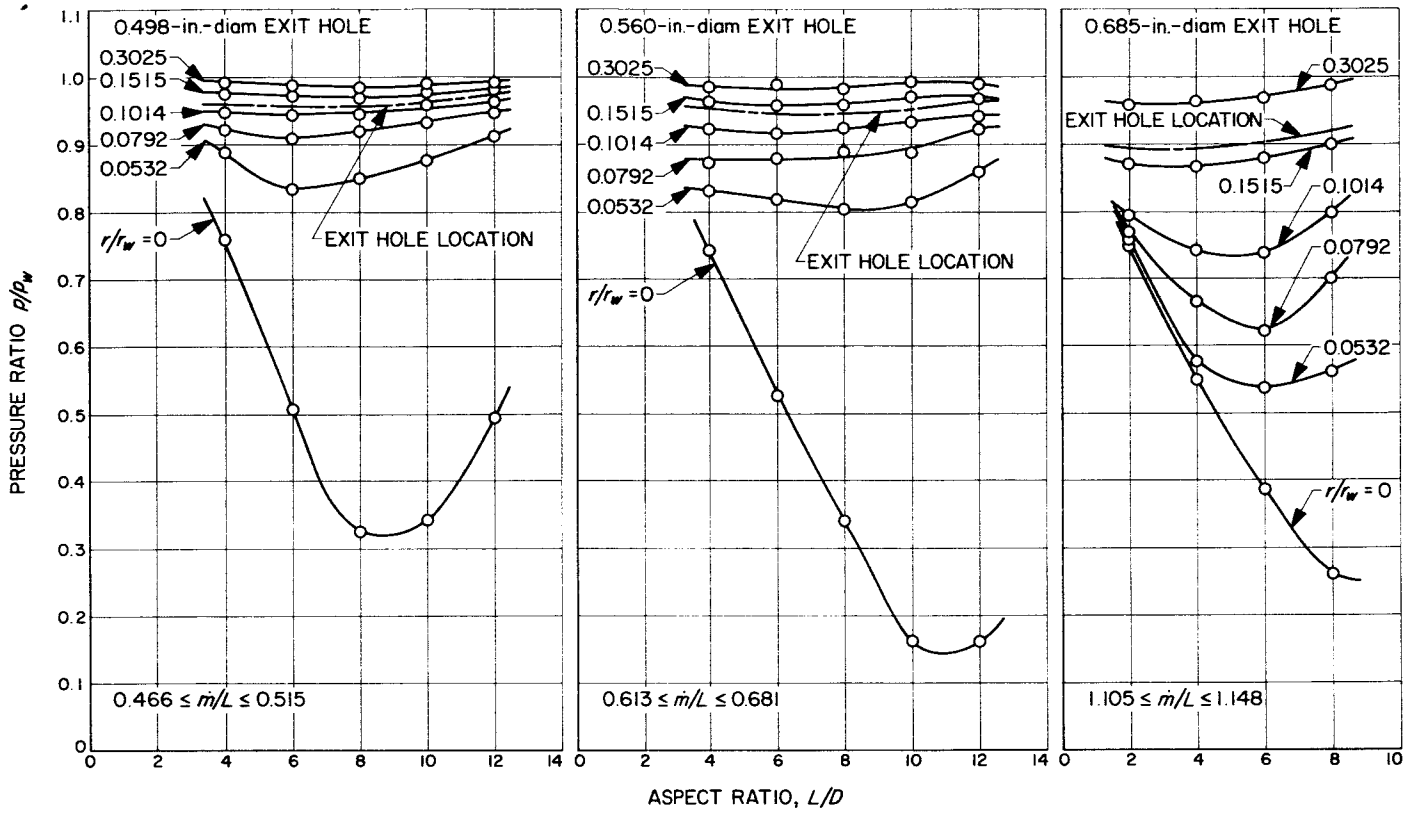

Fig 21. Static pressure at various radial stations—variation with aspect ratio at approximately constant mass flow rate per unit length

integrating the radial momentum equation. A solution for radial distribution of pressure, corresponding to the two-dimensional model of Einstein and Li, is given (Ref. 37) for the region external to the vortex core. This solution is considerably more complicated than the tangential velocity solution, from which it is derived, and its computation is cumbersome.

A more convenient model, with which experimental results may be compared, is the combined vortex, introduced by Rankine many years ago and discussed in various textbooks (e.g., Ref. 57). In this model, different tangential velocity distributions are assumed in two regions, but are matched at some arbitrary reference radius $r_r > 0$; hence, the name, "combined." The vortex core is taken to be solid-body rotation with $v \propto r$, whereas the annular region of the vortex $r > r_r$ is presumed to be potential with $v \propto 1/r$. A modified version of this model with $v \propto 1/r^n$, $n \leq 1$ for $r > r_r$, is presented in the Appendix. Experimental pressure distributions for the smallest exit hole have been compared with this modified model (Fig. 22), where curves for various values of $n \leq 1$ are appropriately labeled. Curves have not been drawn through experimental points (computed using values of r_r and v_w, estimated from the plots of tangential velocity distribution, presented in the next section). An average value of r_r for each L/D was selected to correspond with location of peak tangential velocity. Agreement between model and experimental points is poor, and becomes worse with increasing L/D. It appears that the effective values of n, which merely indicate the degree of departure from a potential vortex, are very low and that n decreases with increasing L/D. Values of center pressure may still be very low, using a model with a low value of n, if r_r is very near to the vortex axis.

Values of pressure-difference ratio $\theta = (p_w - p_c)/(p_r - p_c)$ computed for the smallest exit hole are shown (Fig. 23). Point groupings labelled by aspect ratio L/D are plotted at the same values of reference radius used in Fig. 22. Larger values of θ indicate that a decreasing portion of vortex pressure difference $(p_w - p_c)$ occurs in the vortex core, as compared to smaller values of θ. For fixed L/D, θ increases with p_w, or $\dot{m}/L$. The trend of data with L/D is not easily explained but may be related to presence, or absence, of an air core, as will be discussed later. For comparison, θ curves for the combined vortex with various values of exponent n have been

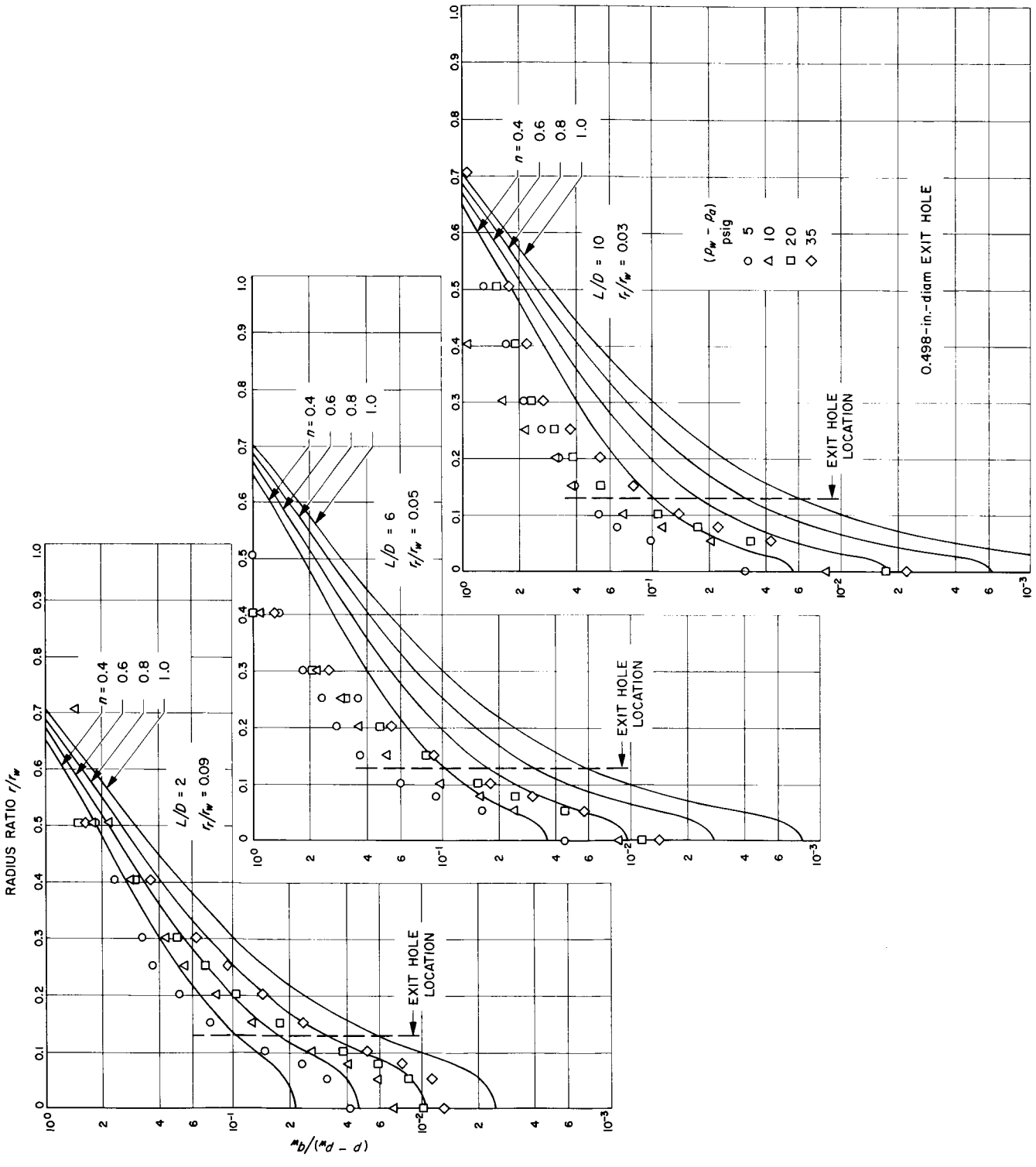

Fig. 22. Radial pressure distributions at closed end-wall—comparison with combined vortex solutions

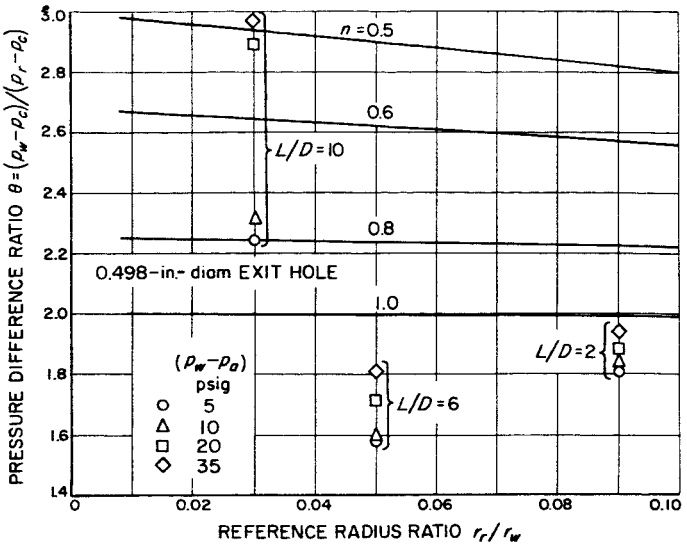

Fig. 23. Experimental values of pressure difference ratio and comparison to combined vortex

included in Fig. 23 (see Appendix). Since experimental results for $L/D = 2, 6$ would indicate a theoretical $n > 1$, it is obvious this particular technique of determining average or effective n applicable to the annular region of a real vortex flow would be of dubious value.

A separate experiment was performed to investigate in more detail the effects of L/D and $\dot{m}/L$ on vortex center pressure p_c. Only p_{tc}, p_c and $\dot{m}/L$ were measured in this experiment, using nominal ½-in.-diameter exit hole. More attention than usual was given to obtaining correct readings of p_c. These results are plotted (Fig. 24). The parameter $(p_{tc} - p_c)/p_{tc}$ is a rough indication of vortex "strength," or circulation outside the core region; it is related to value of $(v/v_{tc})_{max}$ attained in the vortex. Each curve of the family (Fig. 24) has a rather well-defined peak which occurs at successively larger values of L/D, as p_{tc} or $\dot{m}/L$ is increased. An optimum L/D (i.e., that value for which the lowest p_c occurs) exists for each p_{tc}, at least within the L/D range investigated. However, the nature of the tangential velocity data, derived from the static pressure data, prevents concluding that maximum value of v/v_{tc} occurs precisely in coincidence with peak of curves (Fig. 24). It is interesting that the lowest center pressure occurs in rough correspondence to disappearance of the air core in the vortex.

The data of Fig. 24 has been plotted differently in Fig. 25. In this case normalized vortex pressure difference has been plotted vs $\dot{m}/L$ for various constant values of L/D. A decided change in trend with L/D is apparent

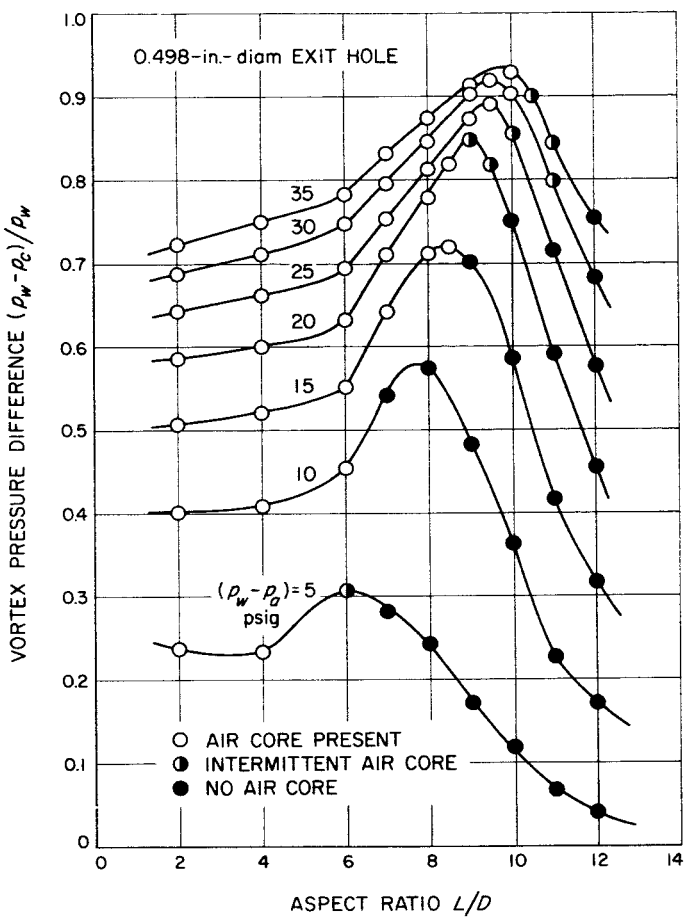

Fig. 24. Variation of vortex pressure difference with aspect ratio for various values of static wall pressure

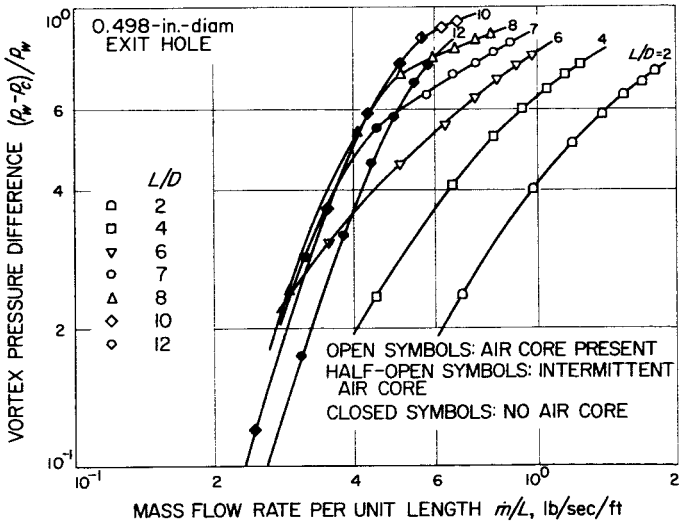

Fig. 25. Variation of vortex pressure difference with mass flow rate per unit length for various values of aspect ratio

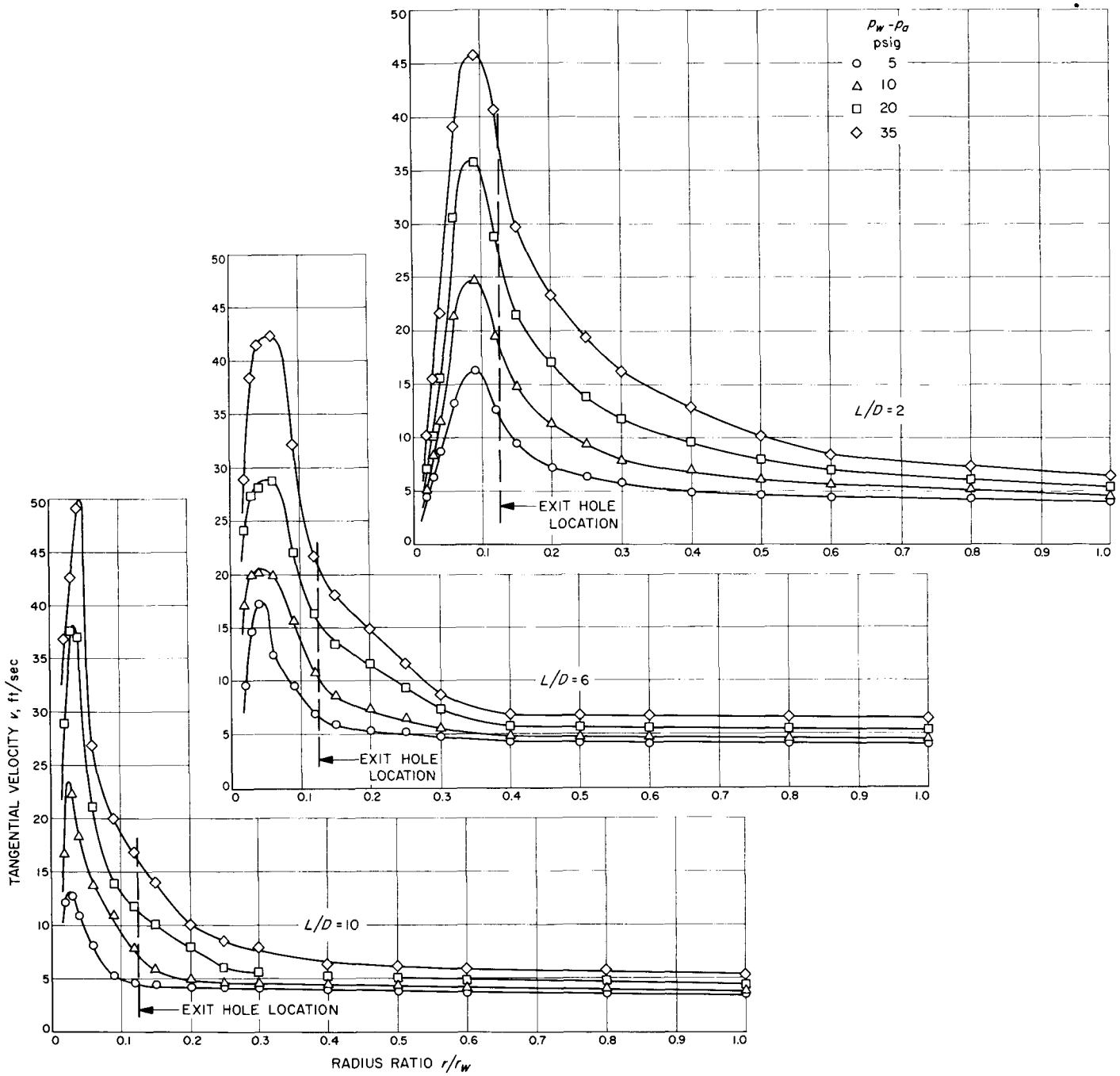

Fig. 26. Tangential velocity distributions for 0.498-in.-diam exit hole

in viewing these curves and seems definitely related to the presence, or absence, of an air core. For $2 \leq L/D \leq 6$ (air core present), $(p_w - p_c)/p_w$ increases with both L/D and $\dot{m}/L$ at a relatively low rate. Curves for $L/D = 7$, 8 appear to represent a transition to a different type of flow; in this region the air core is on the verge of disappearing. At the higher values $L/D = 10$, 12, the curves have a much steeper trend; no air core exists in most of this region. As pointed out previously, one of the more noticeable effects of increasing L/D in the water vortex was a reduction in the vortex core diameter, an observation also verified by flow visualization.

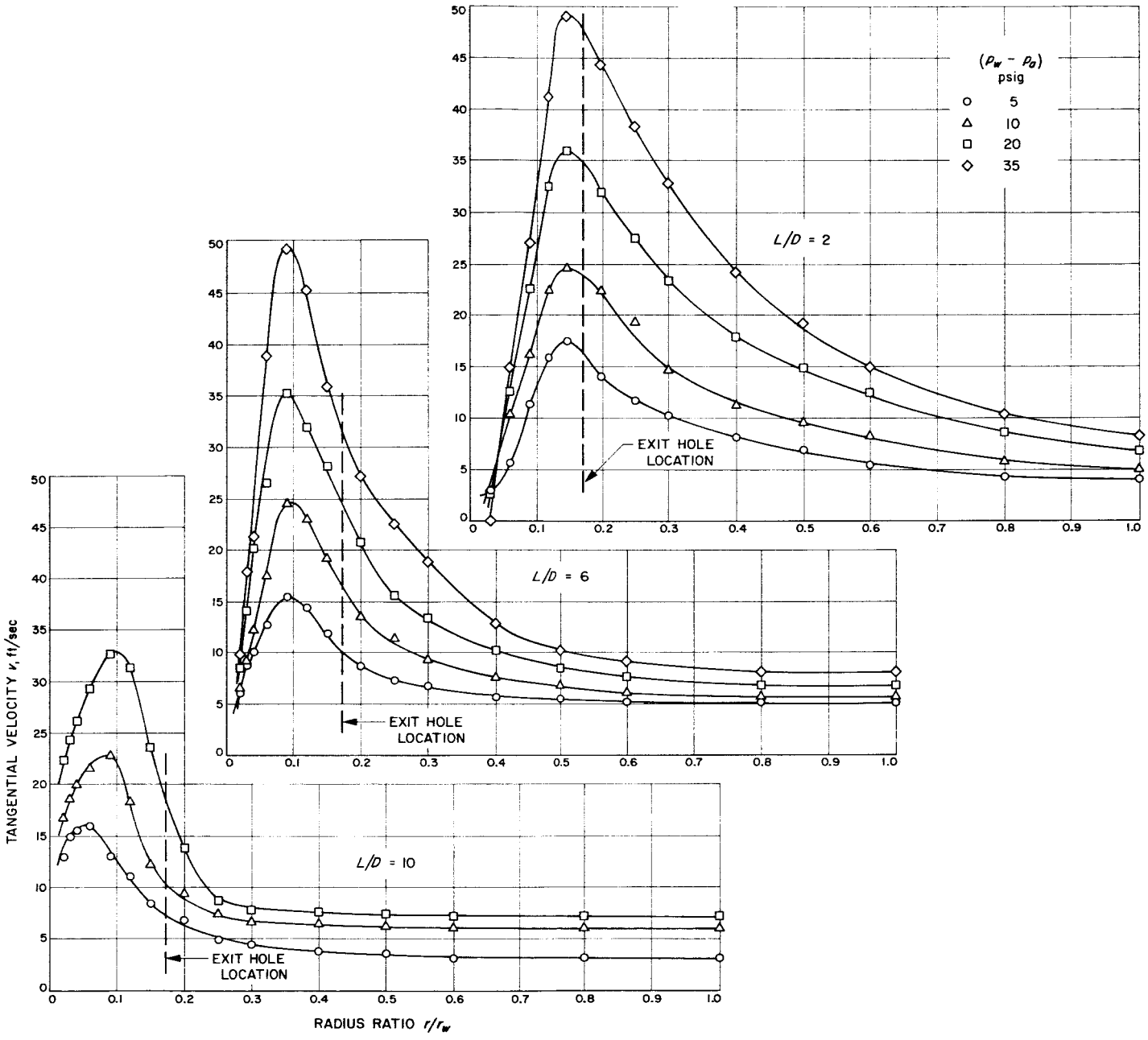

Fig. 27. Tangential velocity distributions for 0.685-in.-diam exit hole

E. Tangential Velocity Determinations

No direct measurements of velocity were made in the water vortex because disturbing effects produced by the probe were considered too serious to ignore. However, tangential velocity was determined by graphical differentiation of radial pressure distributions measured at the closed end-wall and computed according to the simplified radial momentum equation

$$\frac{dp}{dr} = \rho \frac{v^2}{r}$$

or

$$v = \left[\frac{p_{ir} r_*}{\rho} \frac{dp_*}{dr_*} \right]^{1/2}$$

where ρ for water was taken as 62.4 lb/ft^3. Validity of this equation is discussed later. Tangential velocity distributions for three of the five exit holes (Figs. 26, 27

and 28) that correspond to the static pressure distributions are illustrated (Figs. 14, 15 and 16). Maximum tangential velocities of about 50 ft/sec. were achieved. A tabulation of data for these tests is given (Table 1).

Examination of data (Figs. 26, 27 and 28) indicates that maximum tangential velocity increases with increasing $p_w - p_a$ (or $\dot{m}/L$). The radial position of v_{max} (i.e., r_r) is generally less than the geometrical exit-hole radius r_e, but tends to approach r_e as L/D decreases. It is apparent the radial position of v_{max} is more strongly influenced by L/D than by $\dot{m}/L$, an indication L/D exerts a strong effect on vortex core-diameter. This result is clearly seen in Fig. 29, in which the radial position of v_{max}, relative to exit-hole radius, has been plotted as a function of L/D. Each point (Fig. 29) represents an average of four values at different $\dot{m}/L$. The brackets indicate variation within a point group (Table 1).

Figures 30 and 31 show the variation of $(v/v_w)_{max}$ with $\dot{m}/L$, and normalized vortex pressure difference $(p_w - p_c)/p_w$, respectively; data for each exit hole has been plotted separately, with L/D as parameter. Although various curves are not, in some instances, precisely defined, trends appear significant. Thus, $(v/v_w)_{max}$ is found to increase both with $\dot{m}/L$ and $(p_w - p_c)/p_w$. This result, as expected, agrees with theoretical results for two-dimensional, viscous vortex flow (e.g., Ref. 14). The dependence of $(v/v_w)_{max}$ on L/D is reasonably clear on examination (Fig. 30); $(v/v_w)_{max}$ increases with L/D for a fixed $\dot{m}/L$. Less clear is L/D dependence (Fig. 31) at fixed $(p_w - p_c)/p_w$. Thus, $(v/v_w)_{max}$ does not increase uniformly with L/D in this case. Furthermore, the relationship is different for each exit hole.

Aspect ratio also has an effect on the shape of the tangential velocity distributions, especially of small exit

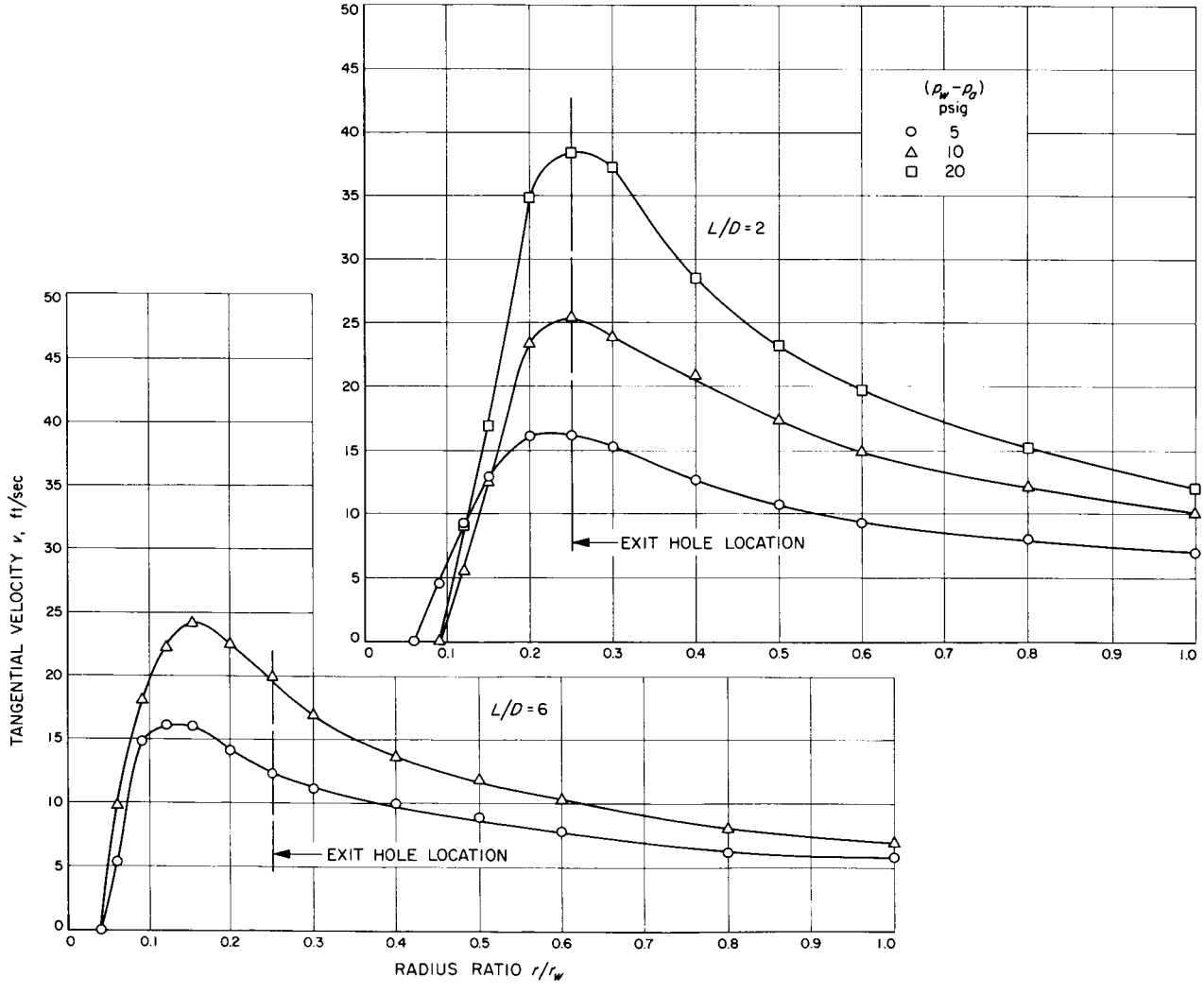

Fig. 28. Tangential velocity distributions for 0.998-in.-diam exit hole

Table 1. Data corresponding to runs for which tangential velocity distributions were determined

Exit hole diam, in.	Experimental conditions				Experimental measurements					Predictions[a]	
	$(p_w - p_a)$ psig	L/D	$\dot{m}/L$ lb/sec/ft	Re_r	$\frac{(p_w - p_c)}{p_w}$	$\left(\frac{v}{v_w}\right)_{max}$	$\frac{r_r}{r_w}$	$\frac{r_r}{r_c}$	$v_* r_*$ at $r_r *$	$\frac{r_r}{r_0}$	$Re_{r,r}$
0.498	5	2	0.760	179.3	0.235	4.05	0.090	0.72	0.364	1.05	2.30
	10		1.078	254	0.406	5.47	0.085	0.68	0.465	0.955	2.75
	20		1.513	357	0.601	6.67	0.085	0.68	0.567	0.87	3.30
	35		2.002	472	0.746	7.11	0.090	0.72	0.640	0.81	3.85
	5	6	0.349	78.8	0.276	4.29	0.045	0.36	0.257	1.33	1.70
	10		0.512	115.5	0.491	4.55	0.040	0.32	0.227	1.25	1.80
	20		0.738	166.6	0.657	5.38	0.050	0.40	0.215	1.07	2.21
	35		0.988	223	0.805	6.58	0.060	0.48	0.296	1.005	2.50
	5	10	0.235	54.6	0.126	3.92	0.025	0.20	0.176	1.40	1.62
	10		0.355	82.5	0.319	6.35	0.025	0.20	0.222	1.27	1.75
	20		0.508	118	0.641	8.69	0.035	0.28	0.127	1.13	2.05
	35		0.692	161	0.837	9.46	0.045	0.36	0.237	0.97	2.58
0.685	5	2	1.148	271	0.251	4.35	0.150	0.87	0.653	Indeterminate	
	10		1.623	383	0.423	4.96	0.150	0.87	0.745	Indeterminate	
	20		2.260	533	0.612	5.28	0.150	0.87	0.793	Indeterminate	
	35		2.703	638	0.744	6.02	0.155	0.90	0.934	Indeterminate	
	5	6	0.640	148	0.282	3.02	0.090	0.53	0.278	1.20	1.90
	10		0.928	214	0.664	4.30	0.090	0.53	0.387	1.03	2.37
	20		1.309	302	0.701	5.18	0.100	0.58	0.518	0.96	2.75
	35		1.743	403	0.850	6.05	0.090	0.52	0.545	0.89	3.19
	5	10	0.467	108	0.366	5.15	0.060	0.35	0.515	1.08	2.19
	10		0.672	156	0.543	3.78	0.080	0.46	0.303	1.02	2.08
	20		0.975	226	0.776	4.55	0.100	0.58	0.273	0.97	2.66
0.998	5	2	2.295	397	0.246	2.35	0.225	0.90	0.529	0.95	2.80
	10		2.532	541	0.406	2.51	0.250	1.00	0.627	0.833	3.63
	20		3.280	774	0.586	3.19	0.260	1.04	0.830	Indeterminate	
	5	6	1.227	289	0.259	2.85	0.135	0.54	0.385	1.08	2.19
	10		1.765	416	0.430	3.46	0.150	0.60	0.519	1.00	2.70

[a] By comparison with the solution of Einstein and Li, Ref. 14.

holes. For example, Figs. 26 and 27 illustrate a gradual, smooth rise in velocity, starting with the effective value at the cylindrical wall, v_w, and proceeding radially inward for $L/D = 2$. Progressing to $L/D = 6$, then to $L/D = 10$, velocity distributions become increasingly flattened in a large annular region adjacent to the wall, then rising rather steeply as peak value is approached near the vortex axis. For higher values of $\dot{m}/L$, the peak is approached in two separate jumps (i.e., two sudden increases in slope occur; the peaks become sharper and narrower). Observation of small foreign particles in the water tended to confirm these observations. Radial motion of particles in a vortex flow depends on the difference between drag and centrifugal force. Drag depends on particle velocity relative to the flow, and to particle size and shape; centrifugal force depends on particle mass and radial acceleration. Particles in the annular portion of the vortex generally orbited in a comparatively lazy

manner. Those approaching a relatively well-defined radial position were observed to accelerate sharply, before being flung radially outward due to substantial increase in centrifugal force.

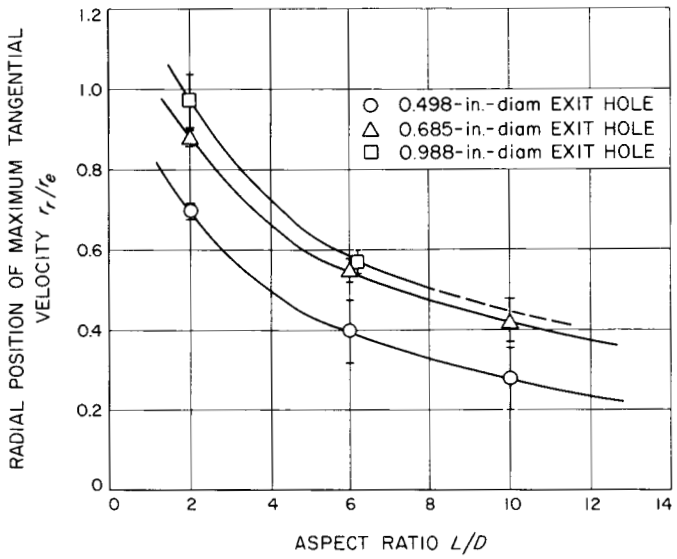

Fig. 29. Variation of position of maximum tangential velocity (relative to exit-hole location) with aspect ratio

Experimental velocity distributions for vortex flows are often compared to two-dimensional models (proposed in Refs. 14 or 34). These laminar solutions for velocity are composed of two parts: one for the core region and one for the annular region of the vortex. They are matched at an arbitrary reference radius r_o that defines the outer edge of the core region. For convenience, r_o is usually assumed identical to exit-hole radius r_e, within which sink-flow is presumed to occur. Comparisons of experimental data with such a theory quickly discloses that (1) r_o and r_e are not the same, and (2) apparent or effective radial Reynolds number is far smaller than indicated by a value based on mass rate of flow through the device. These theories also predict that the tangential velocity peak should occur at $r = r_r = r_o$ when $Re_r \sim 2.5$, $r_r > r_o$ when $Re_r < 2.5$, and $r_r < r_o$ when $Re_r > 2.5$.

Angular momentum distributions for four tests, purposely selected because they have approximately the same radial Reynolds number, are compared to the

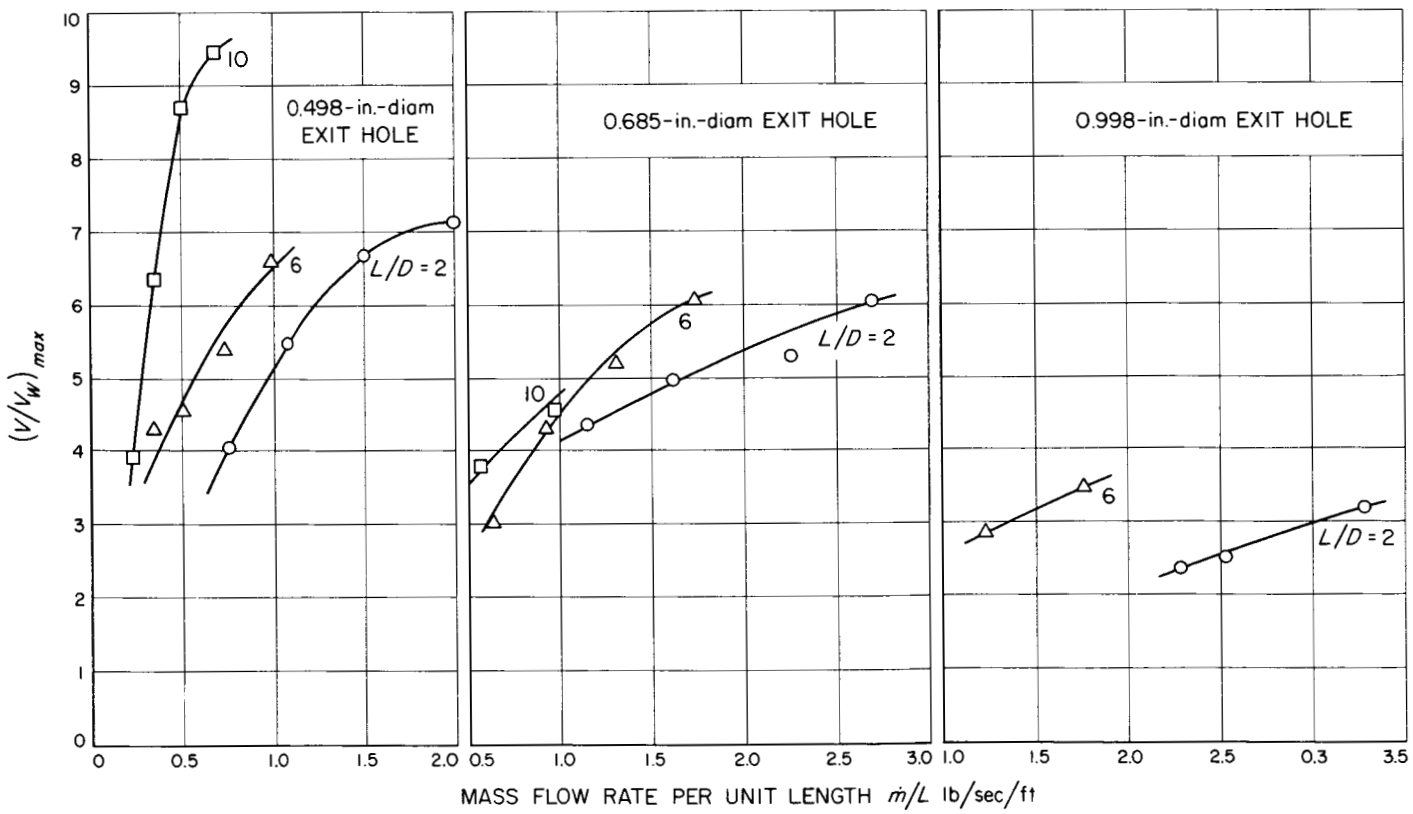

Fig. 30. Variation of maximum value of tangential velocity ratio with mass flow rate per unit length

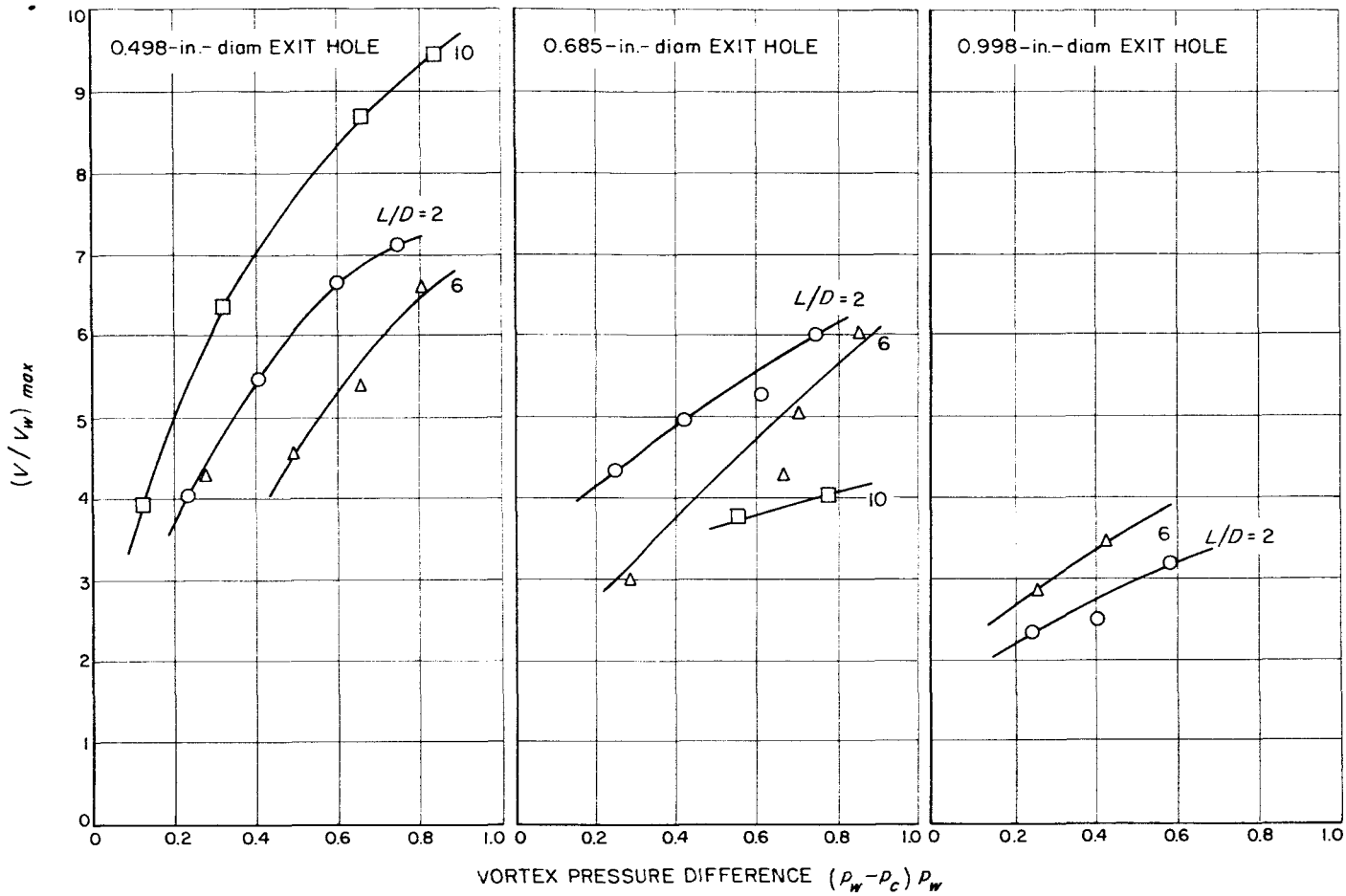

Fig. 31. Variation of maximum value of tangential velocity ratio with vortex pressure difference

Einstein and Li solution (Fig. 32). It became necessary to select an r_o for these test runs and, this was done arbitrarily so that r_o conformed to the approximate edge of the nearly solid-body region of the vortex (selections for r_o; Fig. 32). The experimentally determined angular momentum distributions do not follow the smooth trend (increasing monotonically with r_*/r_{o*}), but rather, appear uneven and erratic. The case shown for $L/D = 10$ is somewhat peculiar in that $v_* r_*$ decays with decreasing r_*, reaches a distinct minimum, and then increases substantially with decreasing r^* until a decay occurs in the core region. Perhaps significant is that the case for $L/D = 6$ exhibits the same behavior, except to a much lesser degree. One explanation for this phenomenon might be that surplus angular momentum furnished by the end-wall boundary layers on eruption from the end walls actually serves to increase angular momentum of the vortex within some limited radial region. Such a possibility is discussed in Ref. 47. An effective radial Reynolds number, approximately $2 < Re_{r,e} < 3$, is indicated by the comparison shown in Fig. 32.

Another way of comparing theory and experiment, thereby determining values of $Re_{r,e}$ for experimental conditions, is to compare only magnitude and position of $(v/v_w)_{max}$—not the shape of velocity distributions. This is done by forcing an agreement of experimentally determined values of both the magnitude and radial position of $(v/v_w)_{max}$ with a theoretical solution so that values of r_o and $Re_{r,e}$ are uniquely determined. When using the Einstein and Li solution, this technique requires either a graphical solution or an iterative procedure for each test. Results of applying this technique to some experimental data are listed in Table 1 and plotted in Figs. 33 and 34. In five of the cases listed (Table 1), solutions or predictions could not be obtained, and these are listed as indeterminate. Individual data points are delineated according to exit-hole size and

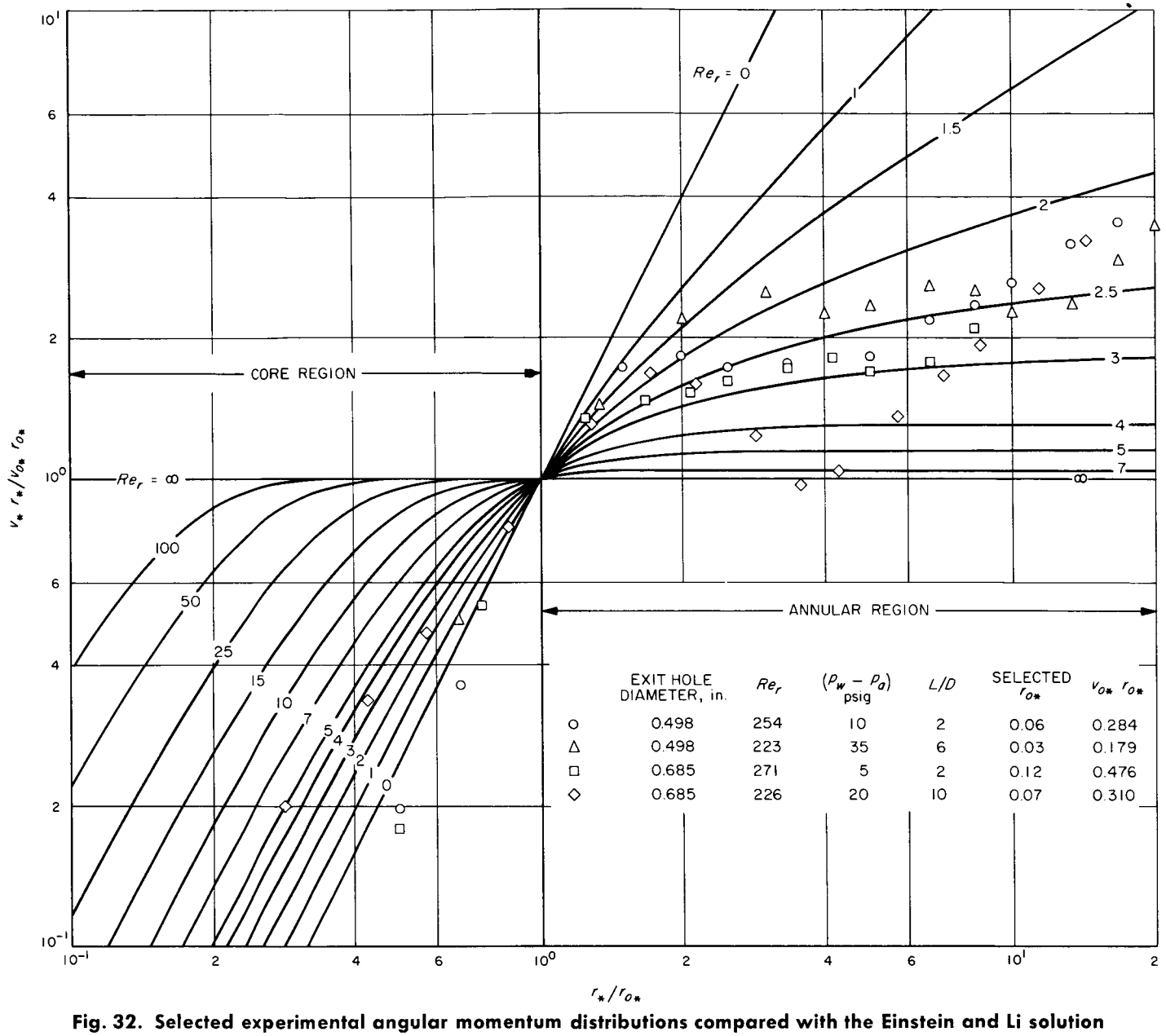

Fig. 32. Selected experimental angular momentum distributions compared with the Einstein and Li solution

L/D (Figs. 33 and 34). The trend of data illustrates that $Re_{r,e}$ increases as Re_r increases (Fig. 33). (Note that the trend of each point group is more clearly defined than the overall trend.) It is probable that an extended range to higher values of Re_r than those obtained would have indicated a leveling-off of this trend, perhaps even a decrease of $Re_{r,e}$ with increasing Re_r. Values of r_o, relative to the position of maximum tangential velocity, are plotted against Re_r (Fig. 34). Again, the trends of point groups are more clearly defined than overall trend of data. Figure 34 illustrates that the position of maximum tangential velocity, which first tends to occur outside the vortex core, shifts inside the vortex core with increasing Re_r. For this data, the cross-over occurs in the approximate range $200 < Re_r < 300$.

F. Further Estimates of Effective Wall Velocity

Interest in determining jet recovery factor $\alpha = v_w/V_j$, tangential Reynolds number $Re_t = \rho v_w r_w/\mu$, and skin friction coefficient C_f at the cylindrical wall for many individual tests, prompted selection of a technique for determining v_w, which was more rapidly and conveniently applied than the graphical differentiation method.

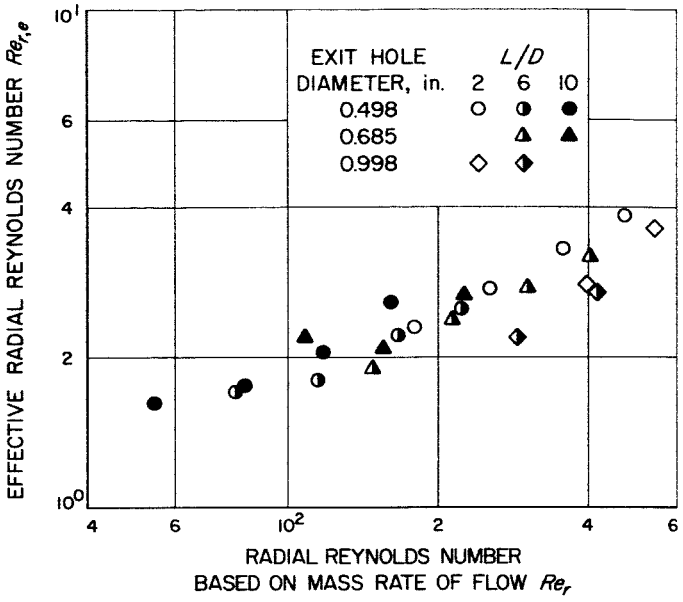

Fig. 33. Prediction of effective radial Reynolds number for vortex flow as obtained by forced agreement of experimental values of magnitude and position of maximum tangential velocity with the Einstein and Li solution

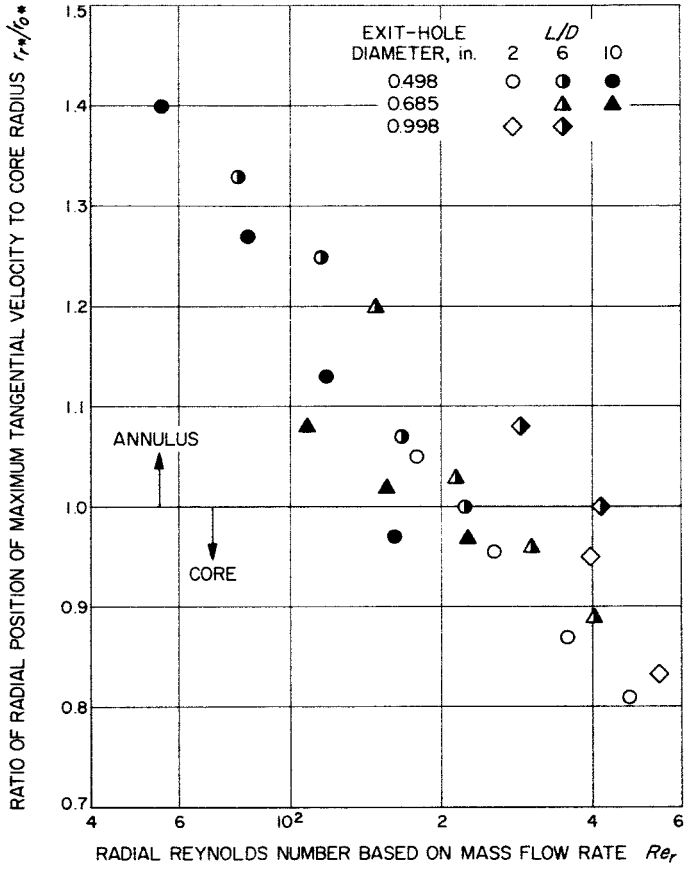

Fig. 34. Prediction of core radius (relative to position of maximum tangential velocity) as obtained by forced agreement between experiment and the Einstein and Li solution

This technique was to fit a pressure distribution for potential flow through two experimentally determined end-wall pressure readings, and to compute v_{w}, which appears as a boundary condition in the resulting equation. The effective tangential wall-velocity, v_{w}, is presumed to occur at the free-stream edge of the cylindrical-wall boundary layer. If one of the selected points for the curve-fitting is located at the cylindrical wall, then v_w is calculated according to

$$v_w = \left[\frac{2(p_w - p)/\rho}{(r_w/r)^2 - 1}\right]^{1/2}$$

for potential flow. The second value of p needed to complete the computation was selected at $r/r_w = 0.506$, one of the end-wall pressure taps. Actual measured values of p at that location were used in each test run, not values obtained by fairing pressure distributions through the point. Several of the 240 test runs were selected to determine how well a potential pressure distribution so derived would fit test data. In most cases the fit was judged adequate to a radius ratio considerably smaller than $r/r_w \sim 0.5$. Initial jet-velocity (V_j) was computed, using measured values of the mass rate of flow and applying the continuity equation to the driving-jet orifices.

Results of applying the procedure just described to the test data are shown in Fig. 35, in which α has been plotted as a function of Re_r (points are distinguished only by exit-hole size). The method of selecting the faired curve through this data (Fig. 35) will be discussed presently. The large amount of scatter evident is caused by inaccuracies in the measured data, and using measured, rather than faired, data for p, at $r/r_w = 0.506$. A least-squares fit of all the data appears as the solid line in Fig. 36; treatment of the data according to exit-hole size appears as the five curves, appropriately labelled. Another least-squares treatment, according to L/D, is shown (Fig. 37). Although the trends and shapes of the curves (Figs. 36, 37) appear roughly the same, differences in level are noticeable, particularly at low Re_r. The up-turn at higher values of Re_r may be misleading, since the number of data points in that region is not large. Theoretically (Ref. 55), one might expect α to increase with increasing Re_r (and hence Re_t) because C_f would decrease correspondingly, but not so sharply as the curves indicate (Figs. 36, 37). A summary of information

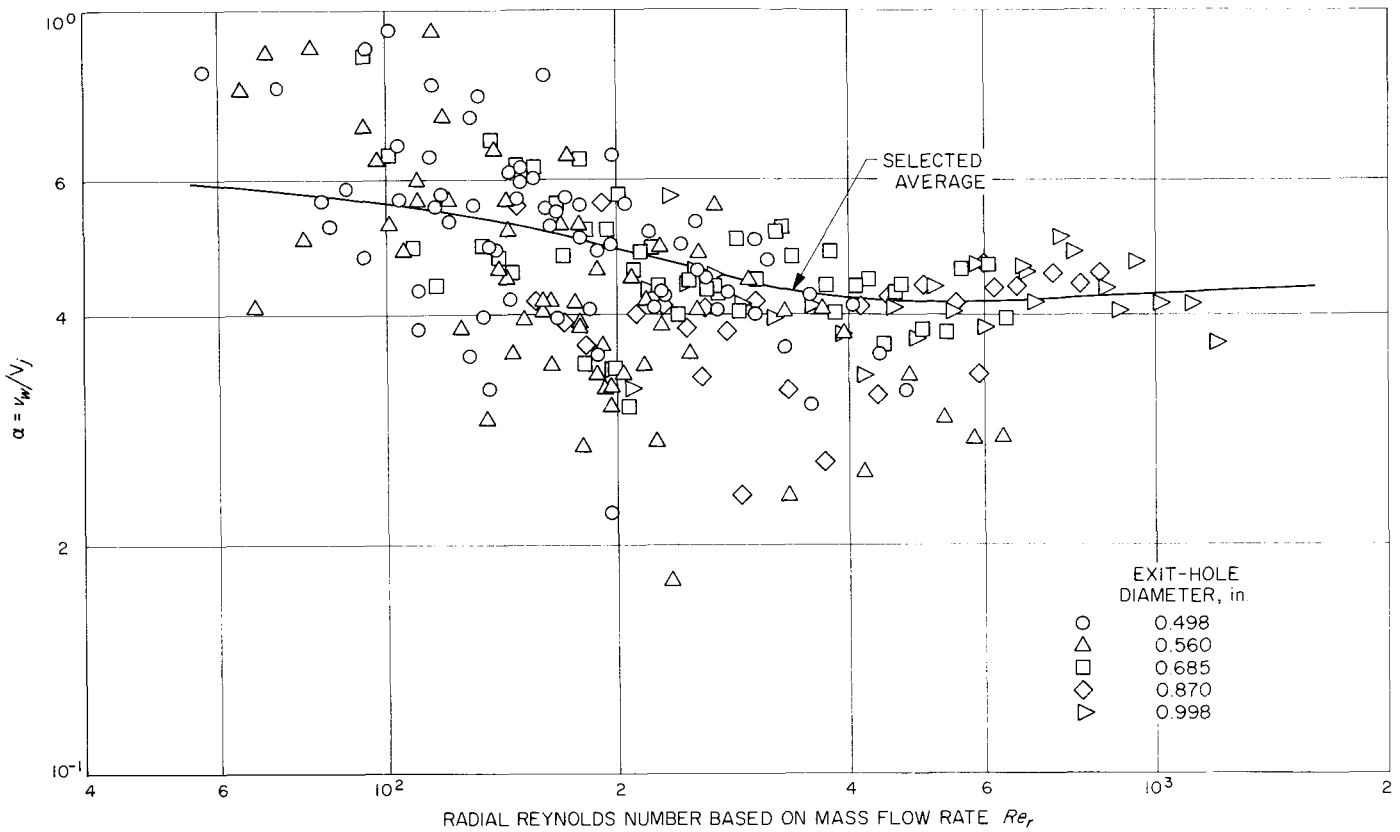

Fig. 35. Jet recovery factor as determined by fitting potential pressure distribution in outer region of vortex

concerning number of test points and standard deviation of α is contained in Table 2.

The large amount of scatter in the data makes it difficult to determine the significance of L/D and exit-hole size. Examination of the total data (Fig. 35) illustrates that most points fall in the region $0.3 < \alpha < 0.6$. The overall fit to all the data (Fig. 36) more closely resembles variations with exit-hole size than variations with L/D. Therefore, it was selected in modified form as most representative of the data. Modification to the overall fit consisted of flattening the curve in the region $Re_r > 250$ (Fig. 35). This treatment is arbitrary, and no attempt is made to justify it on other than intuitive grounds.

The jet recovery factor $\alpha = v_w/V_j$ is significant as a measure of loss of initial momentum driving the vortex because of wall shear and, perhaps, jet mixing. A very low α thus signifies very high viscous losses due to presence of a confining cylindrical wall and poor utilization of available driving momentum. Attempts to improve vortex performance (e.g., by achieving vortexes of significantly greater strength than currently possible) must include a study of workable methods for reducing wall shear. Attempts along this line are reported in Refs. 58 and 59.

It is noteworthy that the method of obtaining v_w described in this section gave consistently lower values than the graphical-differentiation method used in the previous section for determining tangential velocity distributions.

G. Estimates of Tangential Reynolds Number and Cylindrical Wall-Friction

Using values of v_w determined along the lines described in the previous section, values of Re_t can be computed directly from its definition. In the present case, a more convenient method of computation is through use of the relation $Re_t = (\alpha/\phi)\ Re_r$, where ϕ represents the ratio of driving-jet orifice area (or injection area) to total area of the cylindrical wall. For the water vortex apparatus of concern here, $\phi = 0.00197$ and does not vary with L/D. Accepting the functional relation between α and Re_r (the average curve, Fig. 35), the relation between Re_r and Re_t is easily computed, and the solid curve (plotted in Fig. 38) is the result. Included for

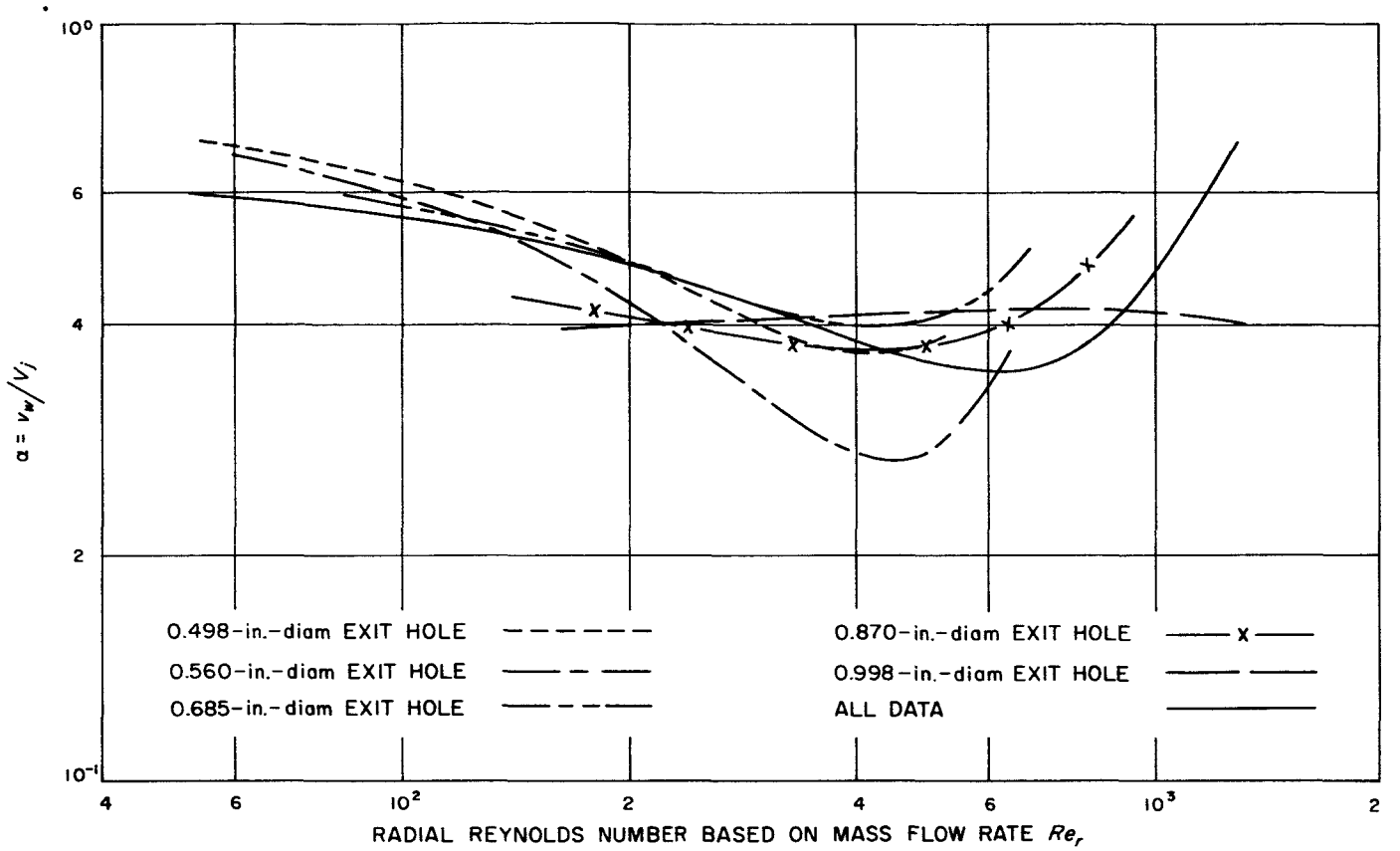

Fig. 36. Jet recovery factor—least-squares treatment of data with point groupings by exit-hole diameter

comparison (Fig. 38) are results predicted by the theory given in Ref. 55; values of C_f, required in that theory, were obtained from flat-plate results (Ref. 56). Curvature, exhibited by the solid curve (Fig. 38) for $Re_r < 400$, is due to the fact that the average α curve (adopted from Fig. 35) decreases with increasing Re_r in that region; a result which is not in agreement with the theoretical relation between α and Re_r (derived in Ref. 55).

A functional relation between α and C_f was developed (Ref. 55) by application of a simple momentum balance applied at the cylindrical wall. Some drawbacks of that analysis were presented there and are not repeated here. It is also true that C_f must in some way depend on Re_t and, in the absence of experimental data for skin friction on the cylindrical walls of vortex tubes, flat-plate results are ordinarily used. Employing the result for α (Fig. 35) again, C_f was calculated, using the relations given in Ref. 55 and plotted against $2\pi Re_t$ (Fig. 39). Hence, C_f may be taken to be the average skin friction coefficient for a flat plate of length $2\pi r_{tc}$. Included (Fig. 39) are the flat-plate results for skin friction (Ref. 56). Although the vortex result (Fig. 39) is inferred from crude data, based on a very simple analysis, the result is of the correct order. If the rising portion of the vortex result is indeed associated with transition from laminar to turbulent flow on the cylindrical wall, the inordinate scatter (Fig. 35) becomes more understandable. There is no reason to believe that α should be strongly influenced by either L/D or exit-hole size, since this would imply those parameters would also exert strong local influence on the cylindrical-wall boundary layer. It is not surprising that the rising portion of the vortex result (Fig. 39), if taken to mean transition, occurs at a lower Reynolds number than an equivalent flat-plate transition. Experimental results (Ref. 60) indicate that early transition can be caused by concave surface curvature.

H. Probe Effects

Difficulties in probing vortex flows, and some of the problems which arise in that connection, are discussed in Refs. 61, 62. It is well known that insertion of a probe into a rotating flow, especially a confined vortex, modifies the original flow in several important ways. These modifications include changes in total mass rate of flow passing through the device and a general rise in static

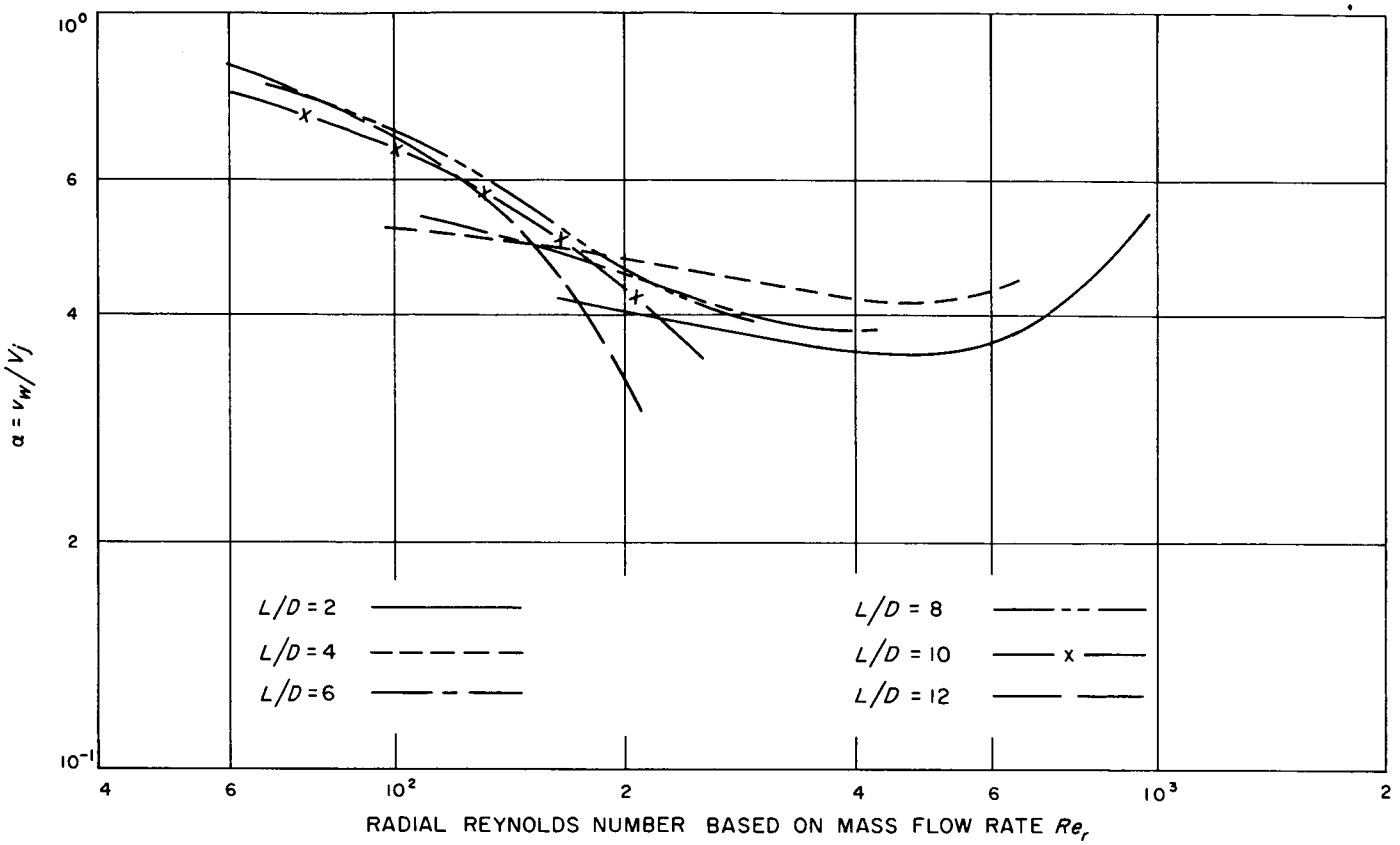

Fig. 37. Jet recovery factor—least squares treatment of data with point groupings by aspect ratio

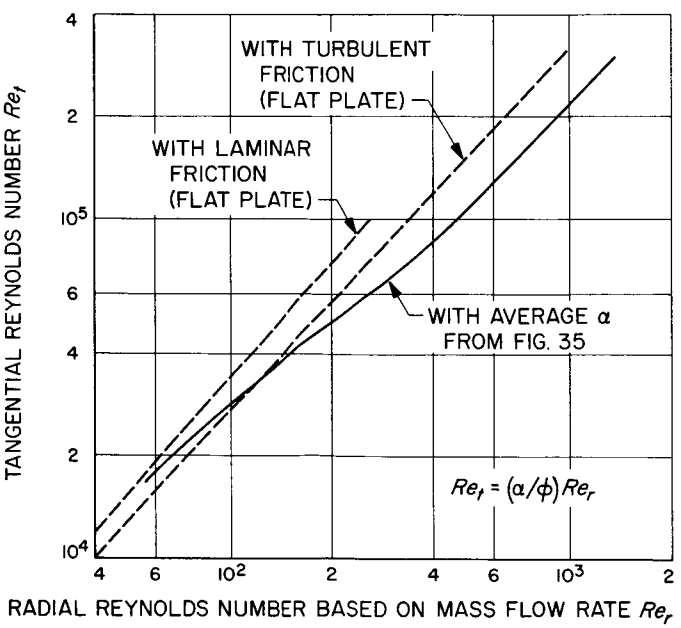

Fig. 38. Relation between Reynolds numbers, using average α, as compared to a theoretical result, using α calculated with flat plate friction

pressure in the central, or core region of the vortex. Both factors contribute to the degradation of the original flow to one that possesses less circulation throughout its radial extent. Unfortunately, little quantitative information on probe effects in vortex flows exists. One experimental technique used (Ref. 62) consists of measuring change in reading, registered by a given probe, on insertion of a second dummy probe into the flow. This method has obvious drawbacks, the most important being that change in the flow field, caused by insertion of the first probe, cannot be determined in this way. In fact, it is the first probe that is responsible for most of the change that occurs. Insertion of a second probe does not produce an additional effect of comparable magnitude. Observations of the end-wall static pressure distribution, particularly in the vortex core region, show this to be true.

The construction of small, cantilever-mounted probes for vortex investigation presents several difficulties. Probes of this type are subject to vibration, especially when inserted near or into the core region of a vortex. The difficulty is to make a probe small enough to mini-

Table 2. Point groupings used in least-squares treatment of jet recovery factor data

Treatment of data by exit-hole size[a]		
d_e, in.	Number of data points	Std. deviation of α
0.498	65	0.120
0.560	63	0.122
0.685	55	0.090
0.870	28	0.065
0.998	29	0.055
Treatment of data by aspect ratio		
L/D	Number of data points	Std. deviation of α
2	34	0.076
4	29	0.062
6	25	0.069
8	21	0.104
10	20	0.149
12	18	0.132
Treatment of entire data[a]		
(Data not distinguished)	Number of data points	Std. deviation of α
	240	0.114

[a] Includes data for odd values of L/D.

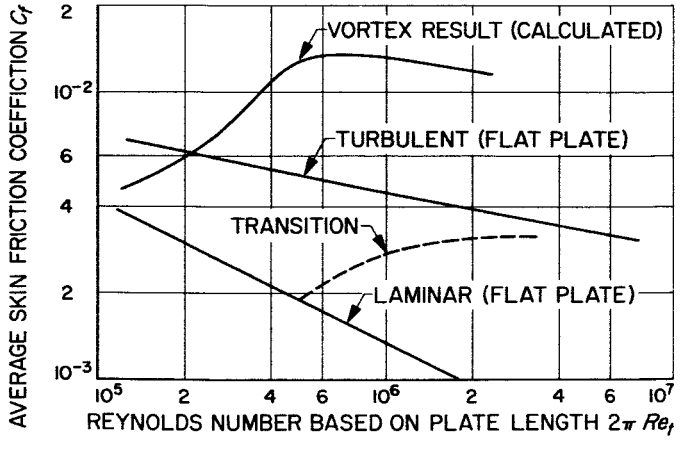

Fig. 39. Comparison of cylindrical-wall friction coefficient for vortex tube, as calculated from average jet recovery results, with flat plate friction results, from Ref. 56

mize flow disturbances, yet sufficiently robust to withstand flow-induced forces. An additional problem of time-response is encountered, which is more serious when using liquid, rather than gas, in a vortex. The type of probe used by Pivirotto (Ref. 12) consisted of a small, hollow tube placed diametrically across the vortex tube and held under tension to prevent distortion in shape. Such a probe is advantageous because it produces a fixed disturbance, which varies only slightly with mass rate of flow, and is apparently independent of axial position. However, experimental data (Ref. 12) show that effect of this type probe is strongly dependent on its diameter.

Flow effects produced by probes of the type just described were investigated briefly in the water vortex. Measurements were made to determine what changes in mass rate of flow were required to maintain a fixed value of pressure at the cylindrical wall, with fixed L/D, using wires of various diameter stretched across a vortex diameter. These results (plotted in Fig. 40) are for wire sizes $\delta = 0.005$, 0.018, 0.035 and 0.050-in. diameters. The wires were located at $L/D = 2$ from the closed end-wall, whereas the vortex, itself, was maintained at $L/D = 5.33$. Points corresponding to the smallest probe-wire deviate from general trends of the curves for a reason not yet established; perhaps that wire was vibrat-

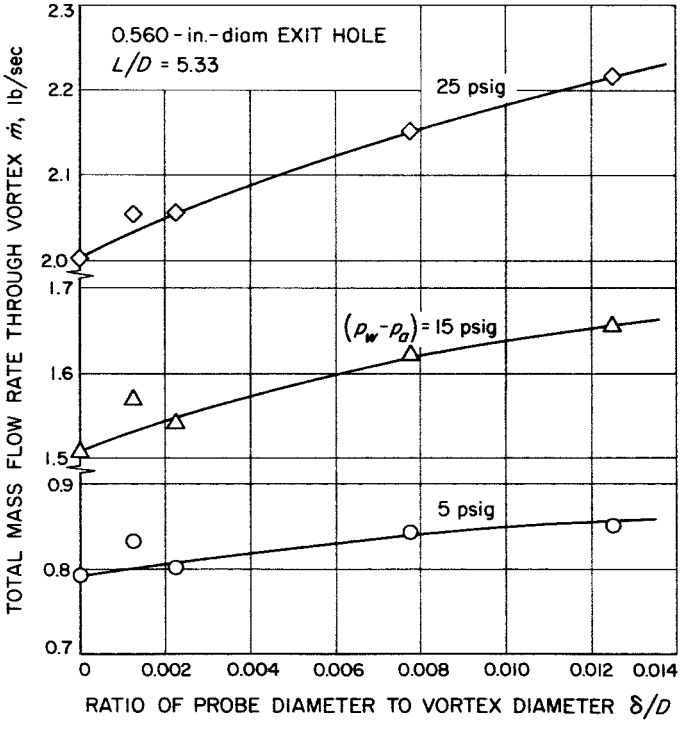

Fig. 40. Effect of probe diameter on mass flow rate

ing excessively, although it did not appear so. Of the wires tested, only the largest was clearly observed to vibrate, and in that case the vibration was also audible.

End-wall pressure distributions were not recorded in this experiment; therefore, no direct comparison with the results (Ref. 12) is possible. However, occasional readings of static center-pressure at the closed end-wall were noted; in each case, the presence or insertion of a wire produced a significant rise in the center pressure p_c. In addition, it was determined that insertion of a second probe at a different axial location did not produce a further change of comparable magnitude.

Data (Fig. 40) were obtained while flow visualization studies were recorded by motion picture photography. These visualization studies indicated that presence of the probe-wire produces pronounced disruption in core flow, greatly retarding axial motion in that region. Other observed effects of the probe-wire were to cause an increase in the core diameter, to generate counterflows not previously present in the vortex, and to greatly retard or eliminate axial flows across the plane of the flow in the annular region of the vortex. The last effect is probably due to the fact that radial in-flow must occur in the wake of the wire because of a tangential velocity defect. The overall effect produced by a probe may be reasoned to be similar to that produced by an end wall, except that the latter effect is more pronounced.

Because of results obtained in studies of probe effects, which are reinforced by the results of Ref. 12, attempts to probe the flow within the water vortex were abandoned.

V. DISCUSSION

The technique of measuring the vortex center pressure (p_c) when an air core was present in the vortex was described previously. Interpretation of this measurement, and its validity, are important to the present work because it had great bearing on the shape and magnitude of the radial static pressure distribution, the radial pressure gradient and, therefore, the tangential velocity in a region near the vortex axis. It is the region near the vortex axis where extremes of these variables are likely to occur. Referring to Figs. 24 and 25, it is not clear whether changes in curve slopes were caused by L/D effects or air core effects. However, it is thought that values of p_c are representative of the center pressure that would have occurred if no air core were present. This remark does not apply for cases in which the air core is obviously impinged on the end wall, e.g., see Fig. 15 (for $L/D = 2$) or Fig. 16; in those instances, gas pressure in the core was undoubtedly measured. Hence, values presented for p_c are probably not values that actually occurred at the vortex axis away from the end wall and within the air core. If an air core rotates as a solid body, within a larger core of liquid that also rotates as a solid body, then the effects of an air core on the surrounding flow should be negligible, except for axial effects. Axial effects may be important if the presence of an air core serves as a restriction within the exit hole, hence a resistance to flow. However, it is suggested that air cores too small to cause impingement on the end wall have negligible effect on the vortex flow or p_c measurements, if proper precautions are taken in the latter measurements.

In most real vortex flows $u \ll v$, so that terms involving u in the radial momentum equation are generally discarded. Examination of the radial momentum equation in cylindrical coordinates indicates that axial variations in velocity are unlikely to be significant compared to the pressure term and the radial acceleration term. Hence, for axisymmetric flow, the radial momentum equation reduces to $dp/dr = \rho v^2/r$. The terms rejected from this equation are estimated to be only 1% of those retained (Ref. 63). Except for axial flow effects, which are relatively small, there is no mechanism by which an axial pressure gradient can be supported across the end-wall boundary layers. Hence, the equation $dp/dr = \rho v^2/r$ is applied to static measurements made at the closed end-wall to determine tangential velocity distributions, even though the radial component of velocity within the end-wall boundary layer is large compared to the tangential component.

No claim has been made that data presented here, particularly tangential velocity and parameters related to tangential velocity, are of high accuracy. Trends exhibited by the data are thought to be meaningful because

the data appears self-consistent in most cases. Pressure measurements in regions of very high, or very low, radial pressure gradient must be made to within approximately 1% accuracy, if tangential velocity is to be determined to an accuracy of 10 to 20%. Such was not the case in this work. In addition, brief calculation shows that in some of the more extreme experimental cases, pressure differences, amounting to as much as 15% of the cylindrical wall pressure, existed across a pressure tap in the region of highest radial pressure gradient. This fact gives some cause for concern as to interpretation of the reading produced at these taps, because these readings must represent some sort of average value.

When assessing the effects of L/D vortex flows, care must be taken to delineate which of the other parameters was held constant during the tests. Assuming that the exit-hole size is held constant, at least three other possibilities exist: (1) constant p_{iw}, (2) constant $\dot{m}$, and (3) constant $\dot{m}/L$. In the case of constant wall pressure (p_{iw}), neither $\dot{m}$ nor $\dot{m}/L$ remains constant with varying L/D. Intuitively, one might expect that results obtained by holding $\dot{m}/L$ constant with varying L/D might be the simplest to understand and, perhaps, the most meaningful. Some trends in the data produced at varying L/D may appear contradictory if other conditions of the tests are not kept in mind.

VI. SUMMARY AND CONCLUSIONS

Radial distributions of static pressure, measured at the closed end-wall of a nominal 4-in., confined, jet-driven water vortex, have been presented for an aspect ratio range of $0 < L/D < 12$. These experiments covered an approximate radial Reynolds number range of $40 < Re_r < 1100$, with nominal exit-hole diameters varying from ½ to 1 in. Tangential velocity distributions, obtained by graphical differentiation of the pressure distributions for several experimental cases, have been presented to give some indication of the effects of exit-hole size and aspect ratio. An attempt has been made to determine the effective radial Reynolds number ($Re_{r,e}$), the jet-recovery factor ($\alpha = v_{iw}/V_j$), the tangential Reynolds number (Re_t), and an average skin coefficient for the cylindrical wall (C_f) for a limited number of experimental conditions.

Changes in end-wall pressure distribution, produced by increasing L/D at constant, static wall-pressure and fixed exit-hole diameter, tend to resemble those produced by decreasing exit-hole diameter at constant L/D. However, pressure-distribution changes, brought about by varying L/D, were somewhat different, depending on whether $\dot{m}$, $\dot{m}/L$, or p_{iw} had been held constant. In the last case, constant p_{iw}, an optimum L/D (i.e., yielding the lowest pressure at the center of the vortex), was found to exist in the range of $0 < L/D < 12$. This was not clearly true for constant $\dot{m}$ and constant $\dot{m}/L$, indicating that experiments should be extended well beyond $L/D = 12$ to fully assess effects of aspect ratio. It was also found that increases in L/D were accompanied by decreases in the core diameter of the vortex.

The shape of tangential velocity distributions was also found to change as L/D was increased; distributions became progressively flattened in the annular region of the vortex, with increasingly sharp rises toward maximum value. The maximum value of v/v_{iw} was found to increase with both $\dot{m}/L$ and L/D; its radial position also moved inward. Effective values of the radial Reynolds number were several orders of magnitude less than values computed from $Re_r = \dot{m}/2\pi\mu L$.

Use of probes in vortex flows of this type should be avoided because even very small probes have been found to produce significant changes in the original vortex flow. Although it may be possible that appearance of new secondary flows generated by probes does not necessarily mean large changes in tangential velocity or circulation distribution, their presence could alter results in some applications (e.g., separation studies).

It is clear that aspect ratio does have significant effects on the strength of confined vortex flows and merits further experimental investigation to values of L/D much greater than used here, with extension to other fluids—particularly gases. It is probable that scale (physical size), not dealt with in this work, is equally important because of cylindrical wall friction effects. In the analysis of Ref. 4, a nuclear propulsion concept in which several thousand vortex tubes are embodied, L/D values of order 100 are employed. It is envisioned such high values of L/D would have adverse effects on performance of the unit due to (1) markedly insufficient vortex strength (separation and

enrichment capabilities), (2) mass flow and/or pressure limitations imposed by large axial pressure drop and cylindrical wall friction (thrust capability), (3) nozzle-sizing limitations imposed by core shrinkage (fuel-retention capability). In addition, flow stability problems, such as organ-pipe oscillations, could be present.

APPENDIX

Pressure Relations for the Combined Vortex, Incompressible Flow

If the possible presence of an air core is disregarded, pressure relations for the modified combined vortex are found by integration of the radial momentum equation $dp/dr = \rho v^2/r$. Tangential velocity is assumed to be a function of radial coordinate only, $v \propto 1/r^n$ where $n \leq 1$; all axial and circumferential variations are neglected. Solutions for the core and annular regions of the combined vortex (Fig. A-1) are matched at an arbitrary reference radius r_r, which is the location of maximum tangential velocity. Starred quantities denote normalization of these quantities with respect to their value at the cylindrical wall.

1. Annular Region, $r_r \leq r \leq r_w$, $n \leq 1$

Boundary Condition: $p = p_w$ at $r = r_w$

Integration yields

$$p = p_w - \frac{\rho v_w^2}{2n}\left(\frac{1}{r_*^{2n}} - 1\right) \tag{A-1}$$

At $r = r_r$, Eq. (A-1) is merely

$$p_r = p_w - \frac{\rho v_w^2}{2n}\left(\frac{1}{r_{r*}^{2n}} - 1\right) \tag{A-2}$$

Or, since $v_w r_w^n = v_r r_r^n$ (A-3)

$$p_r = p_w - \frac{\rho v_r^2}{2n}\left(1 - r_{r*}^{2n}\right) \tag{A-4}$$

2. Core Region, $0 \leq r \leq r_r$, $n = -1$ ($n \leq 1$ in annulus)

Boundary Condition: $p = p_r$ at $r = r_r$

Integration yields

$$p = p_r - \frac{\rho v_r^2}{2}\left(1 - \frac{r_*^2}{r_{r*}^2}\right) \tag{A-5}$$

At $r = o$, Eq. (A-4) reduces to

$$p_c = p_r - \frac{\rho v_r^2}{2} \tag{A-6}$$

3. Summary of Pressure Relations, $q = \rho v^2/2$

Annulus:

$$\frac{(p - p_w)}{q_w} = -\frac{1}{n}\left(\frac{1}{r_*^{2n}} - 1\right) \tag{A-7}$$

Core:

$$\frac{(p - p_w)}{q_w} = -\frac{1}{r_{r*}^{2n}}\left[\theta - \left(\frac{r_*}{r_{r*}}\right)^2\right] \tag{A-8}$$

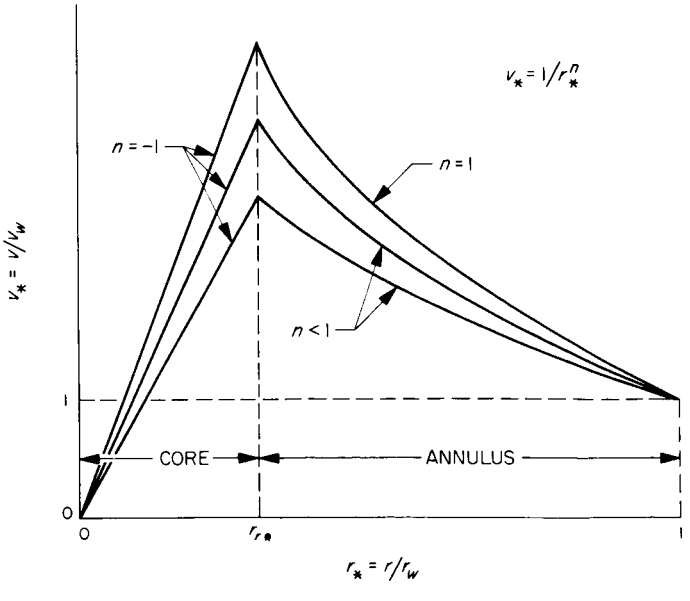

Fig. A-1. Modified combined vortex

where

$$\theta = \frac{(p_w - p_c)}{(p_r - p_c)}$$

The pressure difference ratio θ, which represents the ratio of the total pressure difference across the vortex in the radial direction to the pressure difference across the core, is easily found by combining Eqs. (A-4) and (A-6). Thus,

$$\theta = \frac{(p_w - p_c)}{(p_r - p_c)} = 1 + \frac{1}{n}\left(1 - r_{r*}^{2n}\right) \qquad \text{(A-9)}$$

(A-9) is plotted (Fig. A-2). For a given reference radius r_r, the portion of total pressure difference occurring in the core decreases with decreasing n. When $n = 1$, $\theta \to 2$ as $r_r \to 0$. The last result is in agreement with that given (Ref. 57) for an unbounded vortex, $r_w = \infty$, with $n = 1$ in the annular region $r_r \leq r \leq \infty$.

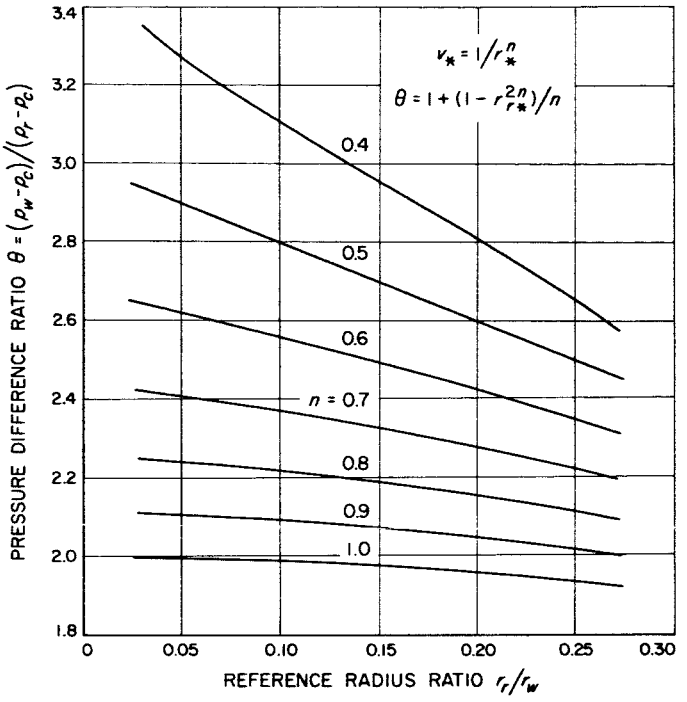

Fig. A-2. Pressure difference ratio for combined vortex

NOMENCLATURE

- C_f skin friction coefficient at cylindrical wall, average value over circumference of vortex tube
- d diameter, general; also diameter of driving-jet orifice
- D diameter of vortex tube
- L length of vortex tube
- $\dot{m}$ total mass flow rate (throughput)
- n exponent in relation vr^n = constant
- p static pressure, absolute
- q dynamic pressure, $pv^2/2$
- r radius, general
- r,θ,z polar coordinates; radial, angular, and axial, respectively
- Re_r radial Reynolds No. based on mass flow rate $(=\dot{m}/2\pi\mu L)$
- $Re_{r,e}$ effective radial Reynolds number
- Re_t tangential Reynolds number $(=\rho v_w r_w/\mu)$
- s spacing distance between driving-jet orifices
- u,v radial and tangential velocity components, respectively
- V_j injection or driving-jet velocity
- x distance from driving-jet orifice, rectilinear case
- α jet recovery factor $(=v_w/V_j)$
- δ probe diameter
- ϵ factor representing relative ripple in axial direction due to a velocity field created by series of parallel jets from holes in-line (see text)
- θ pressure difference ratio $= (p_w - p_c)/(p_r - p_c)$
- μ dynamic (molecular) viscosity
- ρ fluid density
- ϕ ratio of total injection area to total cylindrical surface area

Subscripts

- a ambient or atmospheric conditions
- c value at vortex centerline
- e value at radial position of exit hole
- j refers to jet or injection
- o value at outer edge of vortex core
- r reference radius value, position of maximum tangential velocity
- w value at cylindrical wall (or edge of free stream in the case of tangential velocity)
- $*$ value normalized with respect to its value at cylindrical wall
- max maximum value

REFERENCES

1. Gartshore, I. S., *Recent Work in Swirling Incompressible Flow,* Aeronautical Report LR-343, National Research Council of Canada, Ottawa, June 1962.
2. Rouse, H., "On the Role of Eddies in Fluid Motion," *American Scientist,* Vol. 51, No. 3, September 1963, pp. 285–314.
3. Kücheman, D., "Report on the I.U.T.A.M. Symposium on Concentrated Vortex Motions in Fluids," *Journal of Fluid Mechanics,* Vol. 21, Pt. 1, January 1965, pp. 1–20.
4. Kerrebrock, J. L., and Meghreblian, R. V., "Vortex Containment for the Gaseous-Fission Rocket," *Journal of Aerospace Science,* Vol. 28, No. 9, September 1961, pp. 710–724.
5. Keyes, J. J., Jr., *An Experimental Study of Flow and Separation in Vortex Tubes with Application to Gaseous Fission Heating,* Paper No. 1516-60, presented at the ARS 15th Annual Meeting, Washington, D.C., December 5–8, 1960. (See also *ARS Journal,* Vol. 9, September 1961, pp. 1204–1210.
6. Rosenzweig, M. L.; Lewellen, W. S., and Kerrebrock, J. L., *The Feasibility of Turbulent Vortex Containment in the Gaseous Fission Rocket,* Paper No. 1516A-60, presented at the ARS 15th Annual Meeting, Washington, D.C., December 5–8, 1960.
7. Davis, W. C., et al., *Research and Development on a Vortex MHD Power Generator,* Final Report ER-4737, Thompson Ramo Wooldridge Inc., TAPCO Div., Cleveland, Ohio, December 1961.
8. Elco, R. A.; Hughes, W. F., and Young, F. J., "Theoretical Analysis of the Radial Field Vortex Magneto-gas Dynamic Generator," *Zeitschrift für Angewandt Mathematik und Physik,* Vol. 13, 1962, p. 1.
9. Vonnegut, B.; Moore, C. B., and Harris, C. K., Stabilization of a High-Voltage Discharge by a Vortex," *Journal of Meteorology,* Vol. 17, 1960, pp. 468–471.
10. Tempelmeyer, K. E., and Rittenhouse, L. E., "Vortex Flow in Arc Heaters," *AIAA Journal,* Vol. 2, No. 4, April 1964, pp. 766, 767.
11. Kendall, J. M., *Experimental Study of a Compressible Viscous Vortex,* Technical Report 32-290, Jet Propulsion Laboratory, Pasadena, Calif., June 1962.

REFERENCES (Cont'd)

12. Pivirotto, T. J., *An Experimental and Analytical Investigation of Concentration Ratio Distributions in a Binary Compressible Vortex Flow,* Technical Report 32-808, Jet Propulsion Laboratory, Pasadena, Calif., March 15, 1966.

13. Roschke, E. J., *Flow Visualization Studies of a Confined, Jet-Driven Water Vortex,* Technical Report 32-1004, Jet Propulsion Laboratory, Pasadena, Calif. (to be published September 15, 1966).

14. Einstein, H. A., and Li, H., "Steady Vortex Flow in a Real Fluid," *1951 Proceedings, Heat Transfer and Fluid Mechanics Institute,* Stanford University, Palo Alto, Calif., June 1951.

15. Kelsall, D. F., "Study of Motion of Solid State Particles in a Hydraulic Cyclone," *Transactions of the Institute of Chemical Engineers,* Vol. 30, No. 2, 1952, pp. 87–104.

16. Talbot, L., "Laminar Swirling Pipe Flow," *Journal of Applied Mechanics,* Vol. 21, No. 1, 1954, pp. 1–7.

17. Long, R. R., "Sources and Sinks at the Axis of a Rotating Liquid," *Quarterly Journal of Mechanics and Applied Mathematics,* Vol. 9, Pt. 4, 1956, pp. 385–393.

18. Binnie, A. M., Hookings, G. A., and Kamel, M. Y. M., "The Flow of Swirling Flow Through a Convergent-Divergent Nozzle," *Journal of Fluid Mechanics,* Vol. 3, Pt. 2, December 1957, pp. 216–274.

19. Rao, B. M., "Back Flow in a Vertical Shaft Conveying a Rotating Fluid," *Proceedings of the 5th Congress of Theoretical and Applied Mechanics,* Roorkee, India, 1959, pp. C.157–C.172.

20. Binnie, A. M., and Kamel, M. Y. M., "Experiments on the Flow of Water in a Tube at High Rates of Swirl," *Houille Blanche,* Vol. 14, No. 3, May–June 1959, pp. 348–360.

21. Weske, J. R., and Rankin, T. M., *Production of Secondary Vortices in the Field of a Primary Vortex,* Technical Note BN-244, University of Maryland, Institute for Fluid Dynamics and Applied Mathematics, College Park, April 1961.

22. Nissan, A. H., and Bressan, V. P., "Swirling Flow in Cylinders," *A.I. Ch. E. Journal,* Vol. 7, No. 4, December 1961, pp. 543–547.

23. Sibulkin, M., "A Note on the Bathtub Vortex," *Journal of Fluid Mechanics,* Vol. 14, Pt. 1, September 1962, pp. 21–24.

24. Schulz-Jander, B., *Determination of the Flow Field in a Confined Vortex Chamber,* M.S. Thesis, Rice University, Houston, Texas, May 1963.

25. Turner, J. S., and Lilly, D. K., "The Carbonated-Water Tornado Vortex," *Journal of Atmospheric Sciences,* Vol. 20, No. 5, 1963, pp. 468–471.

26. White, A., "Flow of a Fluid in an Axially Rotating Pipe," *Journal of Mechanical Engineering Science,* Vol. 6, No. 1, January 1964, pp. 47–52.

27. Ross, D. H., *An Experimental Study of Secondary Flow in Jet-Driven Vortex Chambers,* Report ATN-64 (9227)-1, Aerospace Corporation, El Segundo, Calif., January 1964.

REFERENCES (Cont'd)

28. Binnie, A. M., "Annular Hydraulic Jumps," *Proceedings of the Royal Society of London, Series A*, Vol. 282, November 1964, pp. 155–165.

29. Roschke, E. J., "Preliminary Experiments on a Jet-Driven Toroidal Vortex," *Space Programs Summary 37-35*, Vol. IV, Jet Propulsion Laboratory, Pasadena, Calif., February 29, 1964, pp. 76–81.

30. Roschke, E. J., "Some Effects of Aspect Ratio on the Flow in a Confined Jet-Driven Water Vortex," *Space Programs Summary, No. 37-31*, Vol. IV, Jet Propulsion Laboratory, Pasadena, Calif., February 28, 1965, pp. 178–186.

31. Chanaud, R. C., "Observations of Oscillatory Motion in Certain Swirling Flows," *Journal of Fluid Mechanics,* Vol. 21, Part 1, January 1965, pp. 111–127.

32. Rott, N., "On the Viscous Core of a Line Vortex," *Zeitschrift für Angewandte Mathematik und Physik,* Vol. 9b, 1958, pp. 543–553.

33. Long, R. R., "Vortex Motion in a Viscous Fluid," *Journal of Meteorology,* Vol. 15, 1958, pp. 108–112.

34. Rietma, K., and Krajenbrink, H. J., "Theoretical Derivation of Tangential Velocity Profiles in a Flat Vortex Chamber—Influence of Turbulence and Wall Friction," *Applied Science Research,* Section A, Vol. 8, 1959, pp. 177–197.

35. Donaldson, C. duP., and Sullivan, R. D., "Behavior of Solutions of the Navier-Stokes Equations for a Complete Class of Three-Dimensional Viscous Vortices," *Proceedings, Heat Transfer and Fluid Mechanics Institute,* Stanford University, Palo Alto, Calif., June 1960.

36. Long, R. R., "A Vortex in an Infinite Viscous Fluid," *Journal of Fluid Mechanics,* Vol. 11, Pt. 4, December 1961, pp. 611–624.

37. Webb, E. K., "Sink Vortices and Whirlwinds," *Proceedings, 1st Australasian Conference on Hydraulics and Fluid Mechanics,* University of Western Australia, December 1962 (R. Silvester, Editor, Macmillan Co., New York, 1964), pp. 473–483.

38. Thompson, J. F. Jr., *The Structure of Free and Confined Turbulent Vortices,* Research Note No. 44, Mississippi State University, Aerophysics, Dept., State College, Mississippi, May 1963.

39. Gartshore, I. S., *Some Numerical Solutions for the Viscous Core of an Irrotational Vortex,* Aeronautical Report LR-378, National Research Council of Canada, Ottawa, Canada, June 1963.

40. Lewellen, W. S., "A Solution for Three-Dimensional Vortex Flows with Strong Circulation," *Journal of Fluid Mechanics,* Vol. 14, Pt. 3, 1962, pp. 420–432.

41. Lewellen, W. S., "Linearized Vortex Flows," *AIAA Journal,* Vol. 3, No. 1, January 1965, pp. 91–98.

42. Anderson, O. L., *Theoretical Solutions for the Secondary Flow on the End Wall of a Vortex Tube,* Report R-2494-1, United Aircraft Corporation, Research Laboratories, East Hartford, Conn., 1961.

43. Mack, L. M., *The Laminar Boundary Layer on a Disk of Finite Radius in a Rotating Flow, Part I: Numerical Integration of the Momentum-Integral Equations and Application to the Results to Flow in a Vortex Chamber,* Technical Report 32-224, Jet Propulsion Laboratory, Pasadena, Calif., May 1962.

REFERENCES (Cont'd)

44. Mack, L. M., *The Laminar Boundary Layer on a Disk of Finite Radius in a Rotating Flow, Part II: A Simplified Momentum-Integral Method*, Technical Report 32-366, Jet Propulsion Laboratory, Pasadena, Calif., January 1963.

45. Rott, N., *Turbulent Boundary Layer Development on the End Walls of a Vortex Chamber*, Report ATN-62(9202)-1, Aerospace Corporation, El Segundo, Calif., July 1962.

46. Rott, N., and Lewellen, W. S., *Boundary Layers in Rotating Flows*, Report ATN-64(9227)-6, Aerospace Corporation, El Segundo, Calif., September 1964.

47. King, W. S., and Lewellen, W. S., "Boundary-Layer Solutions for Rotating Flows With and Without Magnetic Interaction," *Physics of Fluids*, Vol. 7, No. 10, October 1964, pp. 1674–1680.

48. Rosenzweig, M. L.; Lewellen, W. S., and Ross, D. H., "Confined Vortex Flows With Boundary-Layer Interaction," *AIAA Journal*, Vol. 2, No. 12, December 1964, pp. 2127–2134.

49. Ross, D. H., *An Experimental Investigation of Turbulent Shear in Jet-Driven Vortex Chambers*, Report ATN-64(9227)-5, Aerospace Corporation, El Segundo, Calif., October 1964.

50. Donaldson, C. duP., and Williamson, G. G., *An Experimental Study of Turbulence in a Driven Vortex*, Report ARAP-TM-64-2, (AFOSR 64 1924), Aeronautical Research Associates of Princeton, Princeton, New Jersey, July 1964.

51. Rietma, K., "Liquid-Solids Separation in a Cyclone. The Effect of Turbulence on Separation," *Proceedings, Symposium on the Interaction Between Fluids and Particles, London* (Published by Institute of Chemical Engineering, London), June 1962, pp. 275–281.

52. Knystautas, R., "The Turbulent Jet From a Series of Holes in Line," *Aeronautical Quarterly*, Vol. 15, February 1964, pp. 1–28.

53. Stratford, B. S.; Jawor, Z. M., and Golesworthy, G. T., *The Mixing With Ambient Air of a Cold Airstream in a Centrifugal Field*, Report M. 355, Great Britain Ministry of Aviation, National Gas Turbine Establishment, Farnborough, Hunts, England, June 1962.

54. McLafferty, G. H., *Friction Coefficient Between a Rotating Gas and the Surface of a Containing Tube*, Report M. 1686-6, United Aircraft Corporation, Research Laboratories, East Hartford, Conn., September 1960.

55. Roschke, E. J., "Some Gross Effects of Cylindrical Wall-Friction and End-Wall Boundary Layer Flow on Confined Vortex Flows," *Space Programs Summary 37-21*, Vol. IV, June 30, 1963, pp. 102–108.

56. Schlichting, H., *Boundary Layer Theory*, Pergamon Press, New York, 1955, pp. 108, 146, 438, 439.

57. Prandtl, L., and Tietjens, O. G., *Fundamentals of Hydro- and Aeromechanics*, Engineering Societies Monographs, Dover Publications, New York, 1957, pp. 213, 214.

58. Rosenzweig, M. L., *Velocity and Shear Reduction in Jet-Driven Vortex Tubes*, Report TDR-594 (1203-01) TN-1, Aerospace Corporation, El Segundo, Calif., March 1961.

REFERENCES (Cont'd)

59. Rosenzweig, M. L., *Propulsion Research Program—Summary of Research in the Field of Advanced Nuclear Propulsion,* Semiannual Technical Report TDR-930 (2210-14) TR-1, Aerospace Corporation, El Segundo, Calif., March 1962.

60. Liepmann, H. W., *Investigation of Boundary Layer Transition on Concave Walls,* NACA Wartime Report W-87, National Advisory Committee for Aeronautics, Washington, D.C. (originally issued February 1945 as Advance Confidential Report 4J28, now declassified).

61. Holman, J. P., and Moore, G. D., "An Experimental Study of Vortex Chamber Flow," *ASME Transactions, Series D—Journal Basic Engineering,* Vol. 83, December 1961, pp. 632–636.

62. Eckert, E. R. G., and Hartnett, J. P., "Measurements of the Energy Separation in a High Velocity Vortex Type Flow," *Proceedings, 4th Midwestern Conference on Fluid Mechanics,* Purdue University, Lafayette, Ind., September 1955, pp. 69–92.

63. Reynolds, A., "On the Dynamics of Turbulent Vortical Flow," *Zeitschrift für Angewandte Mathematik und Physik,* Vol. 12, 1961, pp. 149–158.

ACKNOWLEDGMENTS

A number of people have been particularly helpful in contributing to the completion of this work. The author would like to extend his thanks to Thomas Pivirotto and Paul Massier for their many helpful discussions, and to William Thogmartin, Francis Slover, Ronald French, and Ronald Hunter for their conscientious attention to construction, assembly, and maintenance of apparatus and equipment.